

**POLITECNICO DI TORINO**

**Master of Science in Automotive Engineering**

**Analysis, Assessment and  
Simulation of the Real Driving  
Emissions Legislation**



**Supervisor:**  
Prof. Federico Millo

**Candidate:**  
Andrea Protopapa

**December 2020**

*A mia madre*

# Sommario

Questa tesi di laurea magistrale, in collaborazione con FEV Italia s.r.l. tratta l'analisi e l'applicazione della normativa Real Driving Emissions (RDE), oltre alla simulazione e riproduzione delle emissioni di CO<sub>2</sub> di un Plug-In Hybrid Electric Vehicle (PHEV) su diversi cicli omologativi.

A causa del crescente gap tra emissioni omologative e mondo reale, le procedure d'omologazione sono state aggiornate con l'introduzione del Real Driving testing su strada, con l'obiettivo di ridurre emissioni di CO<sub>2</sub> ed inquinanti. Questi test fanno affidamento sull'uso di una nuova tecnologia, il Portable Emissions Measurement Systems (PEMS), che connesso ad On-Board Diagnostic (OBD) e tailpipe del veicolo permette una misurazione in tempo reale delle emissioni dei gas di scarico.

Insieme all'aumento dell'efficacia delle procedure omologative, la nuova normativa introduce complessità in termini di tecnologie utilizzate, criteri per l'approvazione dei cicli ed esecuzione.

La prima parte di questa trattazione, svolta in FEV Italia s.r.l., ha lo scopo di valutare la nuova normativa; A tal proposito è presentata una dettagliata analisi dei moduli del PEMS e il loro principio di funzionamento, insieme alle difficoltà associate all'esecuzione dei test. Poi si considera un veicolo PHEV,

---

sviluppando un modello quasi-statico su GT-Suite per la simulazione dei cicli omologativi New European Driving Cycle (NEDC), Worldwide Harmonised Light Vehicles Test Procedure (WLTP) ed RDE, confrontando i risultati della simulazione con le emissioni sperimentali ottenute coi test su strada e su chassis dyno.

# Abstract

This master thesis in collaboration with FEV Italia s.r.l. concerns the analysis and application of the Real Driving Emissions (RDE) legislation, along with the simulation and reproduction of the CO<sub>2</sub> emissions of a Plug-In Hybrid Electric Vehicle (PHEV) over different homologation cycles.

Due to the increasing gap between homologation and real word driving emissions, the type approval procedures have been updated with the introduction of real driving on-road tests with the goal of reducing the pollutant and CO<sub>2</sub> emissions. Those tests rely on the usage of a new technology, the Portable Emissions Measurement Systems (PEMS), that connected to the vehicle On-Board Diagnostic (OBD) and tailpipe allows the real time measurement of the vehicle's exhaust gasses.

Along with the increased effectiveness of the type approval procedure, the new legislation introduces complexities in the homologation procedure in terms of technology used, criteria for the cycle compliance and execution.

The first part of this dissertation, carried out in FEV Italia s.r.l., was aimed at assessing the new legislation; indeed a detailed analysis of the PEMS modules and its working principles is preseneted, along with the difficulties related to the test execution. Then a PHEV is considered, implementing a GT-Suite

---

quasi-static model for the simulation of New European Driving Cycle (NEDC), Worldwide Harmonised Light Vehicles Test Procedure (WLTP) and RDE homologation cycles, and comparing the simulation results with the experimental emissions obtained with on road test and on the chassis dynamometer.

# Contents

<b>1</b>	<b>Introduction</b>	<b>21</b>
<b>2</b>	<b>The legislation framework</b>	<b>25</b>
2.1	The NEDC procedure . . . . .	25
2.1.1	Decrease of CO <sub>2</sub> and pollutant emissions limits over the years . . . . .	26
2.1.2	Type approval values vs Real Driving Emissions . . . . .	28
2.2	The WLTP procedure . . . . .	30
2.2.1	The use of WLTP and comparison with NEDC . . . . .	30
2.3	Introduction to RDE using PEMS . . . . .	32
2.3.1	The boundary conditions . . . . .	34
<b>3</b>	<b>On-road RDE testing</b>	<b>37</b>
3.1	The PEMS . . . . .	37
3.1.1	Modules and working principles . . . . .	37
3.1.2	Modules installation . . . . .	41
3.2	Onset of the test . . . . .	44
3.2.1	Pre-Test . . . . .	44
3.2.2	Post-Test . . . . .	45

3.3	Emissions determination . . . . .	46
3.3.1	Corrections . . . . .	46
3.3.2	Instantaneous emissions . . . . .	48
3.3.3	Calculation of the final emissions . . . . .	49
3.4	Verification of the trip dynamics . . . . .	51
3.4.1	Verification of the dynamics through the MAW . . . . .	51
3.4.2	Verification of the dynamics through the calculation of $v_{a,pos}$ and RPA . . . . .	54
3.5	Data analysis and validation . . . . .	55
<b>4</b>	<b>Test cycle simulation</b>	<b>61</b>
4.1	Introduction to the simulation advantages and limits . . . . .	61
4.2	Model setup . . . . .	62
4.3	Controls implemented . . . . .	65
4.4	Cycles simulation . . . . .	66
4.4.1	NEDC simulation . . . . .	66
4.4.2	WLTP simulation . . . . .	78
4.4.3	RDE simulation . . . . .	82
<b>5</b>	<b>Conclusions</b>	<b>87</b>

# Acronyms

ATS	After-Treatment Systems
ECE	Economic Commission for Europe
EUDC	Extra-Urban Driving Cycle
FID	Flame Ionization Detector
GHG	Greenhouse Gases
ICE	Internal Combustion Engines
LDV	Light Duty Vehicle
NDIR	Non-Dispersive Infrared Detection
NEDC	New European Driving Cycle
PEMS	Portable Emissions Measurement Systems
PHEV	Plug-In Hybrid Electric Vehicle
RDE	Real Driving Emissions

RF . . . . .	Result Evaluation Factor
RL . . . . .	Road Load
TA . . . . .	Type Approval
UI . . . . .	User Interface
WLTP . . . . .	Worldwide Harmonised Light Vehicles Test Procedure

# List of Symbols

$\eta_{AV}$	Average engine efficiency
$\rho$	Flow density
$\rho_e$	Density of the exhaust gas [kg/m <sup>3</sup> ] at 0 °C
$C_{dry}$	Dry concentration of a pollutant in ppm or per cent volume
$C_{gas,i}$	Measured concentration of the exhaust component 'gas' in the exhaust [ppm]
$C_{PN,i}$	Measured particle number concentration [# /m <sup>3</sup> ] normalized at 0 °C
$C_{wet}$	Wet concentration of a pollutant in ppm or per cent volume
$F_{aero}$	Aerodynamic resisting force
$F_{grade}$	Grade resisting force
$F_{inertia}$	Inertia resisting force
$F_{roll}$	Rolling resisting force

---

LIST OF SYMBOLS

---

$IC_k$	Ratio of the distance driven with the combustion engine divided by the total trip
$k_p$	Pitot constant
$k_w$	Dry-wet correction factor
$LHV$	Fuel lower heating value
$LM$	Technically permissible laden mass
$M_{CO_2,RDE,k}$	Distance-specific mass of CO <sub>2</sub> [g/km] emitted over the RDE trip
$M_{CO_2,WLTP,k}$	Distance-specific mass of CO <sub>2</sub> [g/km] emitted over the WLTP trip
$m_{fuel}$	Fuel mass
$m_{gas,i}$	Mass of the exhaust component 'gas' [g/s]
$M_{RDE,k}$	Final RDE distance-specific mass of gaseous pollutants [mg/km] or particle number [# /km]
$m_{RDE,k}$	Distance-specific mass of gaseous pollutants [mg/km] or particle number [# /km] emissions, emitted over the complete RDE trip and prior to any correction
$OM$	Vehicle optional mass
$p_s$	Static pressure

---

LIST OF SYMBOLS

$p_T$	Stagnation pressure
$P_{traction}^{>0}$	Positive traction power
$PN, i$	Particle number flux [particles/s]
$q_{mew, i}$	measured exhaust mass flow rate [kg/s]
$RF_k$	Resul evaluation factor
$Torque_{DriverDemand, Sim}$	Simulated driver torque demand
$Torque_{EM, Sim}$	Simulated torque of the EM
$Torque_{ICE, Exp}$	Experimental torque of the ICE
$Torque_{ICE, Sim}$	Simulated torque of the ICE
$Torque_{Total, Exp}$	Total experimental torque
$u_{gas}$	Ratio of the density of the exhaust component 'gas' and the overall density of the exhaust
$UM$	Vehicle curb mass
$v$	Flow velocity



# List of Figures

1.1	Transport sector direct CO <sub>2</sub> emissions in the Sustainable Development Scenario, 2000-2018 [1]. . . . .	22
2.1	NEDC speed and gear profile. . . . .	26
2.2	Divergence of real driving vs type-approval CO <sub>2</sub> emissions over the years for different types of vehicle [2]. . . . .	28
2.3	NO <sub>x</sub> emission comparison over NEDC (blue points) and RDE (green points) in urban and extra-urban conditions [3]. . . . .	29
2.4	WLTP speed and gear profile. . . . .	31
3.1	The PEMS modules. From left image to the right one, from top to bottom: PN, PS, PE, PF, GA, and CC. . . . .	38
3.2	Horiba PEMS installation scheme [4]. . . . .	42
3.3	Drift check report. . . . .	47
3.4	Raw exhaust gas values. . . . .	49
3.5	RF evaluation. . . . .	50
3.6	Window calculation example [5]. . . . .	52
3.7	MAW CO <sub>2</sub> characteristic curve. . . . .	54
3.8	Trip dynamics verification in a report. . . . .	56

LIST OF FIGURES

---

3.9	Trip composition of the first RDE test. . . . .	57
3.10	MAW statistics of the first RDE test. . . . .	58
3.11	GPS altitude and vehicle speed over the first RDE cycle. . . . .	58
3.12	Trip composition of the second RDE test. . . . .	59
3.13	Dynamics of the second RDE test. . . . .	60
3.14	Final emissions comparison between tests with different dynamics. In the upper table a more aggressive driving style is adopted. . . . .	60
4.1	Vehicle’s powertrain scheme [6]. . . . .	62
4.2	Vehicle’s specifications [6]. . . . .	63
4.3	Model layout. . . . .	64
4.4	Information flow in a quasi-static powertrain model [7]. . . . .	65
4.5	NEDC Driver Torque Demand. . . . .	67
4.6	NEDC speed trace profile of the torque split imposition model. . . . .	68
4.7	NEDC Engine torque profile of the torque split imposition model. . . . .	69
4.8	NEDC EM torque profile of the torque split imposition model. . . . .	70
4.9	NEDC battery SOC profile of the torque split imposition model. . . . .	70
4.10	NEDC cumulative fuel consumption profile of the split imposition model. . . . .	71
4.11	NEDC speed trace profile of the ICE torque imposition model. . . . .	72
4.12	NEDC Engine torque profile of the ICE torque imposition model. . . . .	73
4.13	NEDC EM torque profile of the ICE torque imposition model. . . . .	73
4.14	NEDC battery SOC profile of the ICE torque imposition model. . . . .	74
4.15	NEDC cumulative fuel consumption profile of the ICE torque imposition model. . . . .	74
4.16	NEDC speed trace profile of the EM torque imposition model. . . . .	75

## LIST OF FIGURES

---

4.17	NEDC Engine torque profile of the EM torque imposition model.	76
4.18	NEDC EM torque profile of the EM torque imposition model. .	76
4.19	NEDC battery SOC profile of the EM torque imposition model.	77
4.20	NEDC cumulative fuel consumption profile of the EM torque imposition model. . . . .	77
4.21	WLTP Driver Torque Demand. . . . .	78
4.22	WLTP speed trace profile. . . . .	79
4.23	WLTP Engine Torque profile. . . . .	80
4.24	WLTP EM Torque profile. . . . .	80
4.25	WLTP engine speed profile. . . . .	81
4.26	WLTP battery SOC profile. . . . .	81
4.27	WLTP cumulative fuel consumption profile. . . . .	82
4.28	WLTP parameter comparison. . . . .	83
4.29	RDE GPS road elevation profile. . . . .	84
4.30	RDE speed trace profile. . . . .	84
4.31	RDE Engine Torque profile. . . . .	85
4.32	RDE EM Torque profile. . . . .	85
4.33	RDE fuel consumption cumulative. . . . .	86
4.34	RDE SOC profile. . . . .	86



# List of Tables

2.1	NEDC cycle characteristics. . . . .	26
2.2	WLTP vs NEDC cycle characteristics comparison. . . . .	32
2.3	Parameter for RDE compliance. . . . .	34
2.4	Parameter for RDE compliance divided in zones. . . . .	34
3.1	Drift check pollutant boundaries. . . . .	46
4.1	Summary results of all the models for the NEDC simulation. . .	78
4.2	Results of the model for the WLTP simulation. . . . .	82
4.3	Results of the model for the WLTP simulation. . . . .	83



# Chapter 1

## Introduction

Despite the more restrictive legislation limits, the transport sector contribution to the pollutant and Greenhouse Gases (GHG) emissions, such as the CO<sub>2</sub>, remains of crucial impact and its control is needed to avoid a further increase of the global temperature. According to [1], the transportation in 2018 still accounted for 24% of direct CO<sub>2</sub> emissions from fuel combustion. The greatest part of those emissions comes from passenger vehicles which contributed for 45.1%, meanwhile another 29.4% came from trucks carrying freight, as showed in figure 1.1.

To decrease the CO<sub>2</sub> emissions, diesel engines have been developed and widely spread. As the diesel engines became more popular, however, the NO<sub>x</sub> emissions raised with a constant increase in the difference between type approval and actual emissions, highlighting a not effective Type Approval (TA) procedure and an ease in NO<sub>x</sub> emission reduction during the homologation procedure, with the "Dieselgate" as a clear example. According to [8], about half of the cases of premature deaths due to PM<sub>2.5</sub> and Ozone formation attributed to

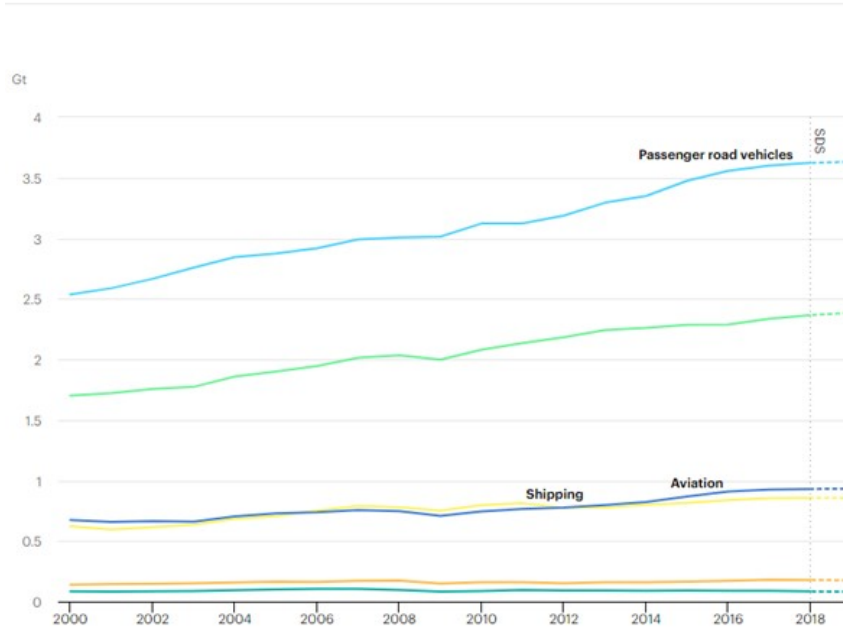


Figure 1.1: Transport sector direct CO<sub>2</sub> emissions in the Sustainable Development Scenario, 2000-2018 [1].

high NO<sub>x</sub> emissions from light duty diesel vehicles in Europe in 2013 could have been avoided if these vehicles had not emitted more than the EU limit value in real driving conditions. To increase the effectiveness of the TA procedures, the outdated New European Driving Cycle (NEDC) cycle has been replaced with the more reliable Worldwide Harmonised Light Vehicles Test Procedure (WLTP) on chassis dynamometer in a first place, and then coupled with the Real Driving Emissions (RDE) tests featuring a Portable Emissions Measurement Systems (PEMS) that allows an on-road measurement of CO<sub>2</sub> and pollutant emissions, avoiding the problems related to the laboratory cycles and increasing the randomness of both cycle trip and environmental conditions. Along with the increased reliability of the TA procedures, however, the RDE test introduces many challenges, from the trip definition and test execution, to

the PEMS installation and checking. The increased complexity of the procedure raised the interest in the simulation field to predict the CO<sub>2</sub> and pollutant emissions prior to the testing. An effective solution to the CO<sub>2</sub> and pollutant reduction is found in the hybridization of the powertrains. According to [9], the hybridization leads to an increase of the Internal Combustion Engines (ICE) efficiency and improved CO<sub>2</sub> emissions with a reduction of up 50% in the urban cycle. In this framework, a comparison between the NEDC, WLTP and RDE TA procedures is carried out, along with an analysis of the technical difficulties that come along with the RDE testing and the development of different models for the simulation and reproduction of the homologation cycles, evaluating the CO<sub>2</sub> emissions of an hybrid vehicle.



# Chapter 2

## The legislation framework

### 2.1 The NEDC procedure

Since the vehicle emissions are dependent on the engine operating conditions, every vehicle has to be tested following a speed-time trace which defines a cycle. Considering the Light Duty Vehicle (LDV) homologation, in EU the cycle used until 2017 had been the NEDC performed on chassis dynamometer. On the chassis dyno the vehicle is blocked with the wheels free to rotate with rolling and aerodynamic resistance reproduced by electric motors as function of the trace speed. This means that a dyno calibration is needed, and it is done by means of the definition of the Road Load (RL) coefficients, obtained experimentally through the Coast-Down test. The exhaust gasses are collected and diluted with air to cool down and avoid any kind of post-reaction and condensation of water. The collected gasses are sampled and analysed to evaluate the pollutant concentration which is function of the engine operating condition. The NEDC is made of 4 Economic Commission for Europe (ECE) cycles

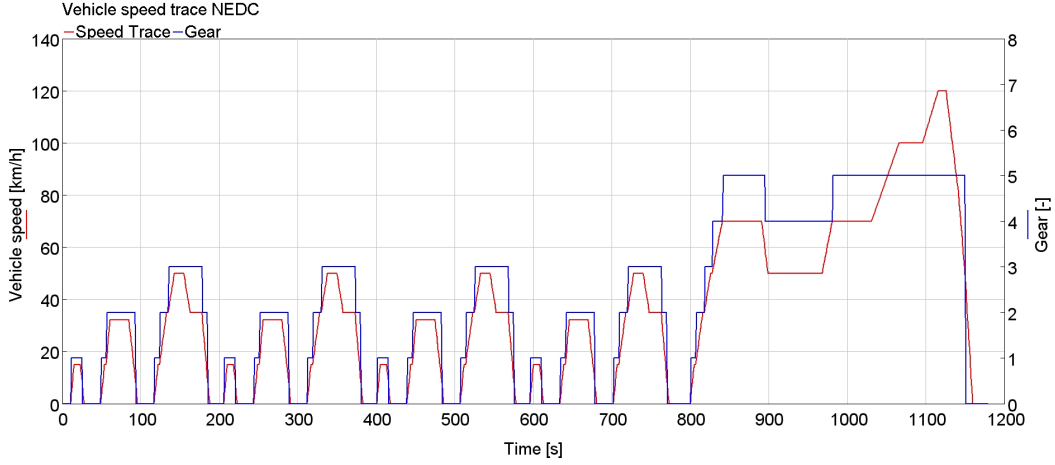


Figure 2.1: NEDC speed and gear profile.

Distance [km]	11.007
Time [s]	1180
Average speed [km/h]	33.6
Max speed [km/h]	120
Idle time [%]	20.7

Table 2.1: NEDC cycle characteristics.

plus 1 Extra-Urban Driving Cycle (EUDC) cycle, and is represented in figure 2.1, and whose characteristics are the expressed in table 2.1. The cycle defines a set of points in which the engine is operated that are concentrated just in a small region of the map, thus bringing several problems discussed in paragraph 2.1.2.

### 2.1.1 Decrease of CO<sub>2</sub> and pollutant emissions limits over the years

The NEDC has been used not just for the measurement of the CO<sub>2</sub>, but for the main vehicle pollutant measurements such as NO<sub>x</sub>, CO, and HC too. During the years, the pollutant limits have been set and cut down according

to the emissions obtained with the best technology currently available, which represent the After-Treatment Systems (ATS) state of art. The limit values are defined by the Euro normative in Europe, with difference between CI and SI engines. The  $\text{NO}_x$ , which is responsible of many secondary pollutants such as acid rain and photochemical smog, is of particular interest for CI engines. The impossibility of the usage of the TWC makes the after treatment of the pollutants in CI more complicated compared to the SI engines. From Euro 5 on, PN restrictions have been added to the CI vehicles limits in terms of mass and then extended, in Euro 6, to SI vehicles due to the direct injection. The limits on the PN has been introduced once a reliable, repeatable and accurate way to measure the particles has been developed. Concerning the GHG reduction, the EU has defined some mandatory emission target since 2009, setting emission performance standards. The ratio between the energy needed to complete a cycle and the energy generated by the fuel combustion defines the average efficiency of the engine according to the equation 2.1 of paper [10].

$$\eta_{AV} = \frac{\int_0^{t_{cycle}} P_{traction}^{>0} dt}{m_{fuel} \cdot LHV} \quad (2.1)$$

Where  $P_{traction}^{>0}$  is the positive traction power,  $m_{fuel}$  is the fuel mass and  $LHV$  is the fuel Lower Heating Value.

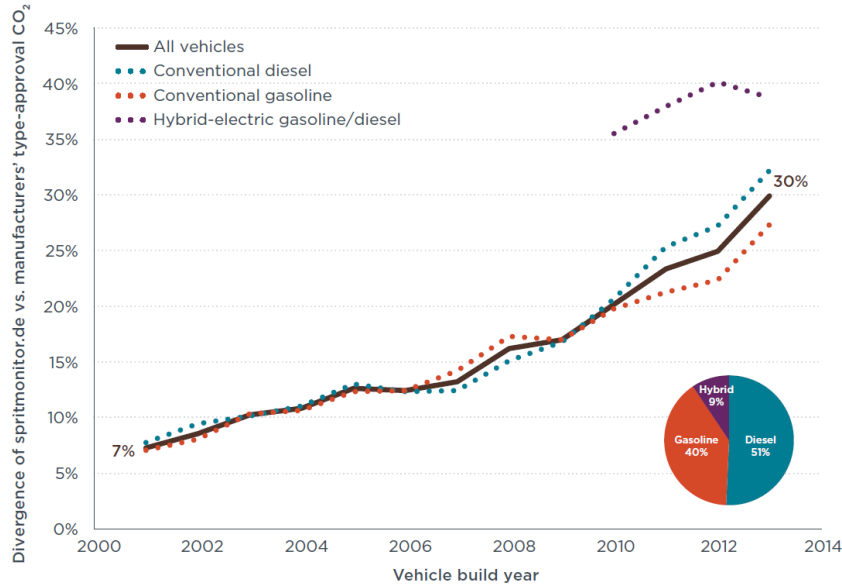


Figure 2.2: Divergence of real driving vs type-approval CO<sub>2</sub> emissions over the years for different types of vehicle [2].

### 2.1.2 Type approval values vs Real Driving Emissions

Despite the reduction of pollutant and CO<sub>2</sub> emissions limits and targets, the regulation applies just to TA emissions measured over the testing cycle. Based on the data of almost 500'000 vehicles, [2] study proves a raising discrepancy between the regulatory improvements and the everyday emissions. According to Spritmonitor.de, an online database that provides on-road fuel consumption figures for car in Germany, the gap raised from 7% in 2001 to 30% in 2013, as shown in figure 2.2.

[3] compares, in figure 2.3, the instantaneous NO<sub>x</sub> emissions over urban and extra-urban driving on chassis dyno NEDC and real driving. The results define an increase of NO<sub>x</sub> levels of the 25% over the urban circuit and emissions doubled during the extra-urban part.

The reason of the NEDC ineffectiveness could be addressed to many factors:

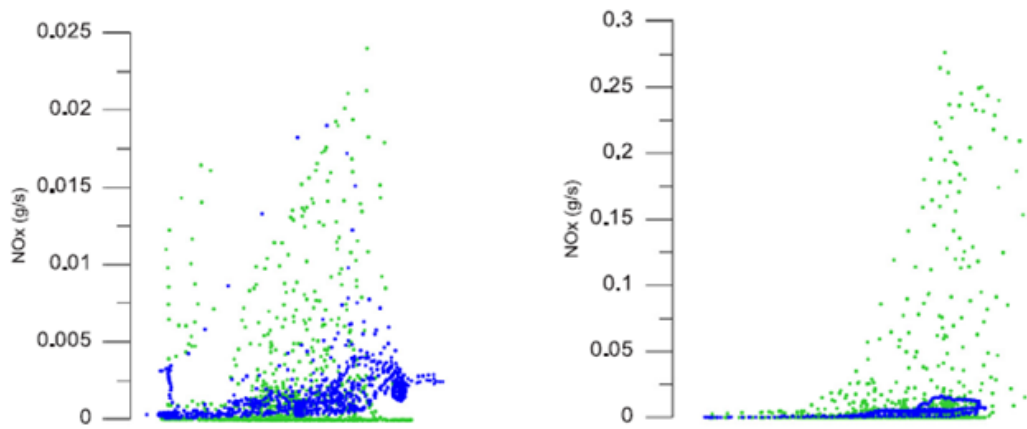


Figure 2.3:  $\text{NO}_x$  emission comparison over NEDC (blue points) and RDE (green points) in urban and extra-urban conditions [3].

- The NEDC is a cycle that does not fit the dynamics of the real driving, with moderate transients and many constant-pedal flat zones which are not representative of real driving conditions.
- The high freedom on aspects of the test procedure such as the coast-down testing for the evaluation of the road loads defined some factors far from the reality.
- The type approval vehicle mass does not consider the optional requirements and the permissible laden mass.
- The type approval cycle does not consider the road gradient and the environmental conditions.
- The concentration of operative points in just a region of the load-rpm map rewards technologies that are not effective along all the map or less effective in the real life compared to the TA procedure. The EGR, for example, is effective in low load-low rpm zones, where a high amount of

recirculating gasses can be introduced. The development of fuel saving technologies e.g. Start and Stop have high benefits just on the NEDC.

## 2.2 The WLTP procedure

### 2.2.1 The use of WLTP and comparison with NEDC

The introduction of the WLTP from the European authorities is an attempt to fill the gap between TA and real-world emissions. The WLTP differs from the NEDC in terms of cycle characteristics and test procedure. Although it is still a laboratory test, the cycle is more dynamic and the test procedure more representative of the actual driving conditions.

The differences between NEDC and WLTC can be listed:

- Evolved requirements in terms of test temperature, test mass and RL. The test mass is no longer obtained as the vehicle's curb mass increased of 100kg, but as function of the optional mass equipment and the permissible laden mass too, as expressed in equation 2.2:

$$TM_H = UM + OM + 100 + 0.15 \cdot (LM - UM - OM - 100) \quad (2.2)$$

Where  $UM$  is the curb mass,  $OM$  is the mass of optional equipment, and  $LM$  is the technically permissible laden mass.

- The driving cycle is represented in figure 2.4 and made of 4 phases: low speed, middle speed, high speed, and ex-high speed. The phases duration

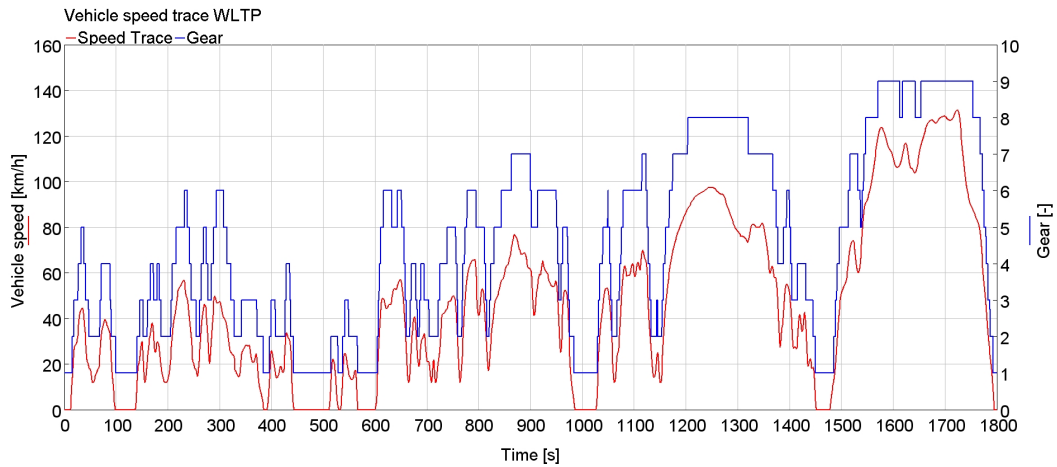


Figure 2.4: WLTP speed and gear profile.

is determined on traffic volume ratios between the phases. A comparison with the NEDC cycle is made in table 2.2.

- The combination of those factors raised the energy demand required to finish the cycle. [10] investigated on the impact of the driving cycle and test procedure on the CO<sub>2</sub> emissions increase from NEDC to WLTP to assess which are the most important factors. The results showed that the primary factor contributing to the CO<sub>2</sub> emissions increase is represented by the more severe test condition (e.g. vehicle test mass and RL) rather than by the more dynamic driving. The energy demand raised of 44% for the SI engine and of 23% for the CI engine.
- The dynamic of the cycle generates points that are spread all over the load-rpm map, covering also zones in which the efficiency of combustion is high and thus increasing the overall efficiency passing from NEDC to WLTP from 25% to 30% for the SI engine and from 27.5% to 32% for the CI engine.

	NEDC	WLTP
Distance [km]	11.0	23.3
Time [s]	1180	1800
Average speed [km/h]	33.6	46.5
Max speed [km/h]	120	131.3
Stop [s]	280	226
Constant Driving [s]	493	98
Acceleration [s]	247	762
Deceleration [s]	539	730

Table 2.2: WLTP vs NEDC cycle characteristics comparison.

Concerning the THC, CO, and NO<sub>x</sub> emissions, [11] investigates on the difference between pollutant emissions of a light-duty vehicle equipped with a Lean NO<sub>x</sub> Trap (LNT) and Diesel Particulate Filter (DPF) ATS over the NEDC and WLTP, considering different ambient temperatures. [12], instead, focused on the effects of different technologies on CO<sub>2</sub> emissions over NEDC and WLTP, developing models for several passenger cars validated against test data. As trend over those technologies, a decrease of the effectiveness during the passage from NEDC to WLTP is present. The reduction of the effectiveness of the Start and Stop (S&S) is related to the longer idling period of the NEDC compared to the WLTP, the reduction of the Brake Energy Recuperation System (BERS) is related to the longer braking period of the NEDC, and the Variable Valve Actuation (VVA) effectiveness loss is related, instead, to the engine operating range, since more effective at lower speed and loads.

## 2.3 Introduction to RDE using PEMS

Although the WLTP represents a good improvement towards a real driving condition, it is still a laboratory cycle thus limited, and can still be optimized.

To minimize the discrepancy between homologation testing and real driving emissions, the idea of moving part of the testing from laboratory to the public roads with the onset of the RDE is adopted. The RDE is an on-road test that requires a PEMS, a new technology that, installed on the vehicle and connected to its OBD and tailpipe, allows the sampling and recording of the vehicle's emissions during a trip. The introduction of an on-road test has obvious advantages related to the assessment of the actual environmental and road slope conditions, avoiding the need of the dyno setting and RL definition, and giving a more robust measurement of the vehicle emissions over a wider range of scenarios. Furthermore, the test's driving dynamics and trip requirements can vary with high degree of freedom, although restricted by some boundary conditions determined by the legislation, preventing cycle cheating. As drawback, instead, the homologation effort required to define a suitable route compliant to the boundary condition is increased, and the cycle suffers of reproducibility problems related to the environmental conditions, the trip adopted, and the driver behaviour. The study conducted by [13] indicates that the same vehicle can provide different energy and emission outcomes for a different trip, driver, and meteorological conditions. Furthermore, the possibility of performing a homologation cycle which is not compliant to the RDE boundary condition, thus not valid, is more likely to happen. The RDE emissions must be compared to the Euro 6 regulatory limit through the conformity factor.

Parameter	Requirement
Payload	Artificial payload may be added until the total payload does not exceed the 90% of the sum of the driver and equipment
Ambient temperature	Moderate conditions: $3^{\circ}C \leq T \leq 30^{\circ}C$ Extended conditions: $-2^{\circ}C \leq T < 3^{\circ}C$ and $30^{\circ}C < T \leq 35^{\circ}C$
Altitude	Moderate conditions: $h \leq 700m$ Extended conditions: $700m < h \leq 1300m$
Vehicle conditioning	The vehicle shall be driven for at least 30 min, parked with doors and bonnet closed and keeping engine-off between 6 and 56 hours.

Table 2.3: Parameter for RDE compliance.

Parameter	Urban	Rural	Motorway
Instantaneous speed	$v \leq 60km/h$	$60km/h < v \leq 90km/h$	$90km/h < v$
Trip composition	29% to 44% of the total trip distance	23% to 43% of the total trip distance	23% to 43% of the total trip distance
Average speed	15 to 40 km/h	60 to 90 km/h	>90 km/h
Stop period	6 to 30% of the time duration of the urban operation but with individual stop periods no longer than 300s		
Distance	> 16km	> 16km	> 16km
Trip duration	90 to 120 min		

Table 2.4: Parameter for RDE compliance divided in zones.

### 2.3.1 The boundary conditions

The RDE test has high degree of freedom but it is limited by a set of boundary conditions on the vehicle payload, preconditioning, ambient conditions, trip requirements and drive dynamics. Those parameters must be chosen according to the legislation and are showed in table 2.3.

Concerning the trip, it is divided in three phases: urban, rural, and motorway, each one with their own characteristics. The most important trip requirements needed for a compliant RDE are expressed in table 2.4.

To monitor those parameters, the PEMS is connected to engine OBD, GPS

and a weather station. For what does concern the dynamics of the test, a separate paragraph is dedicated. [14] investigated on the practical difficulties in the selection of the driving route. According to this study, the more limiting rule associated with the route design is that the vehicle must be driven above 100 km/h for at least 5 min. This means that a sufficiently long motorway zone with a 110 km/h or greater speed limit must be found. Additionally, the traffic unpredictability could be a problem leading to a stopping period which exceeds the limits or to an excess urban operation during the rural sector, thus the rural sector must be carefully evaluated too.



# Chapter 3

## On-road RDE testing

### 3.1 The PEMS

#### 3.1.1 Modules and working principles

The PEMS is a technology made of different modules, working independently, connected to each other and to the engine OBD, GPS, weather station, and vehicle tailpipe. The modules showed in figure 3.1 are divided into:

CC Central Control

PS Power Supply

PE Power Exchanger

PF Pitot Flow

GA Gas Analyser

PN Particle Number



Figure 3.1: The PEMS modules. From left image to the right one, from top to bottom: PN, PS, PE, PF, GA, and CC.

In the following, a brief explanation of the PEMS main components' functioning principle is given:

**The Pitot Tube** The Pitot tube is used to measure the flowrate of sampled exhaust gasses. Although it's not the best measuring system for a pulsating flow [15], typical of internal combustion engines, most of the PEMS feature it since able to measure high-temperature fluids, and represents a good trade-off between costs and advantages. Its working principle is based on the Bernoulli's law, evaluating the flow velocity through pressure difference measurements between the stagnation point  $p_T$  and the static point  $p_s$ , the flow temperature and density  $\rho$ , and a factor  $k_p$ , the Pitot constant, empirically evaluated. The flow velocity is obtained according to equation 3.1.

$$v = k_p \sqrt{\frac{2(p_T - p_s)}{\rho}} \quad (3.1)$$

A high sensitivity differential pressure sensor is then needed to have an accurate

flow measurement. In fact, the flow rate is dependant upon the square root of the pressure difference, traducing in great error for small deltas around the zero value. During the onset of the RDE testing, a Pitot tube of the right diameter must be chosen according to the engine displacement to avoid measurement problems:

- Choosing a Pitot tube smaller than needed would lead to a flow excess, with the tube reaching the critic flow rate and acting as a choke.
- Choosing a Pitot tube larger than the needed one would lead to a difference in pressure which is too low due to the low flow speed, struggling with the differential pressure evaluation and increasing uncertainty on the measurement.

To this purpose, the tubes are divided into typologies according to maximum flow rate admissible, diameter, and engine power and displacement, into:

- Type B: diameter of 40mm, maximum flow rate of 4,5 m<sup>3</sup>/min. Suitable for engines until 1600cc and 120CV.
- Type C: diameter of 60mm, maximum flow rate of 10 m<sup>3</sup>/min. Suitable for greater displacement engines.

**Batteries and power supply** The PEMS is either powered by batteries or the PS. The two 24V, 40Ah batteries, installed in parallel to allow simultaneous discharging, granting from 3.5h to 4h autonomy depending on the environmental conditions, are used during testing. The PS power supply is connected to a 220V energy grid and needed to simultaneously recharge the batteries and supply the PEMS modules.

**The Gas Analyser** In the GA, the probe is heated around  $95^{\circ}\text{C}$ . It analyses the exhaust gasses, measuring the CO and  $\text{CO}_2$  by means of Non-Dispersive Infrared Detection (NDIR), the HC by means of the Flame Ionization Detector (FID), and the NO and  $\text{NO}_x$  exploiting the chemiluminescence reactions.

The NDIR working principle is based on the gas capacity to absorb just part of the infrared radiations at which is exposed, according to its atomic structure. The NDIR instruments are made of an infrared source, two volumes filled with gasses and with transparent bases to allow the rays passage, and two chambers filled with the gas of the CO,  $\text{CO}_2$  and  $\text{O}_2$  type, divided by a membrane that forms one of the two armatures of a capacitor. Of the two volumes, one is filled with the gas to be analysed and the other one with nitrogen as reference gas. If the volume is filled with the pollutant, the gas will absorb part of the ray's energy, thus leaving less energy for the gas inside the chamber to be absorbed and this will generate a membrane deflection traduced into a signal of the pollutant concentration. If the analysed gas does not present the pollutant, then the same amount of energy heats the gas inside the chambers leading to no deflection of the membrane.

Concerning the Flame Ionization Detector (FID), this working principle is based on the strong ionization given by the hydrocarbon combustion compared to the combustion of pure hydrogen. The instrument is made by a burner with a calibrated flux of the analysed gas that passes through a flame made out by the combustion of hydrogen in air. Two electrodes are present near the flame to catch the ions current which is proportional to the presence of HC in the analysing gas.

For the  $\text{NO}_x$  detection, chemiluminescence instruments are adopted. The NO

inside the exhaust gasses combine with the  $O_3$  according to the reaction 3.2:



The above reaction generates  $NO_2$  which is in the excited state. Returning in the normal state it emits radiations that are detected by a photomultiplier with an intensity proportional to the presence of the pollutant. The reaction occurs just with  $NO$ , thus a  $NO_2 / NO$  converter is needed exploiting the reaction 3.3.



Dry air is pumped into the  $O_3$  generator needed for the onset of the reaction [16].

**The Particle Number** The PN probe presents air sample and dilution tubes that draw around 0.7 l/min of exhaust gasses. The PN uses a condensation particle counter that exposes the aerosol to supersaturated vapor, growing particles of the sizes at which they can be optically detected. The droplets go through the focal point of a laser beam, scattering light in a proportional way to the presence of PN [17]. The Horiba PN module uses the isopropyl alcohol as working fluid, which provides excellent condensational growth.

### 3.1.2 Modules installation

If the PN and PS are not present, the other PEMS modules can be installed outside the vehicle and covered with a case, otherwise the PEMS must be

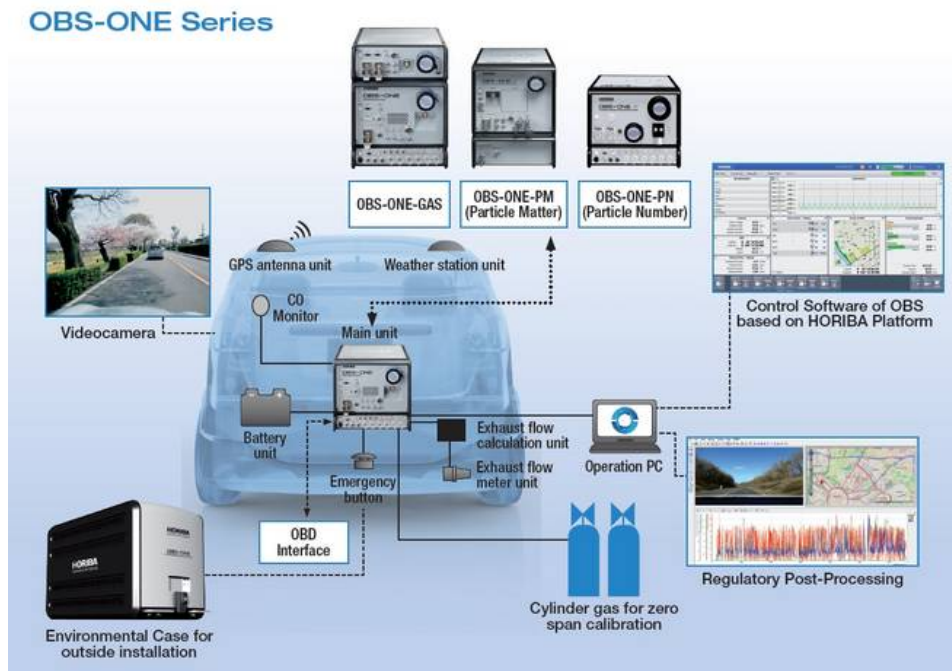


Figure 3.2: Horiba PEMS installation scheme [4].

installed inside the vehicle, protecting the most expensive modules. This solution is preferable since allows an easier drift check post-test that must be performed with a difference in the temperature of the modules before and after the trip not greater than  $5^{\circ}\text{C}$ , although could be challenging to fit all the modules inside cars with small room available. The legislation defines some general rules to be adopted for the proper PEMS installation: in particular refers to the backpressure generated by the sampling probes, that should not affect the pressure at exhaust outlet, and to the exhaust mass flow meter, which is recommended to be properly chosen according to the maximum expected flow rate. The modules' installation scheme of the PEMS used for the tests performed in FEV Italia s.r.l. is showed in figure 3.2.

The PEMS power supply is connected to the PE that distribute the power along the PN and from the PN to the GA. From the GA the power connections

are made through low amperage cables to the CC and PF.

The CC is connected via LAN to the GA, PN, and PC, where all the vehicle and PEMS parameters are displayed through the Horiba User Interface (UI), and via USB to the vehicle OBD. The OBD gives the PEMS information about the engine speed and coolant temperature, and is mandatory for the vehicle homologation. A connection to the GPS and weather station is implemented and needed to obtain reliable measurements. Every time the PEMS is turned on, the CC performs some checks prior to the turning on of the other modules. The GA powers the CC and features connections for the sample and dilution air probes. Additional connections for the Air and Span needed for the calibration and drift check are present, along with the NH<sub>3</sub> filter.

The PN powers the GA and features connections for the sample and dilution air along with the PN filter.

The PF is powered by the CC and connected to the Pitot Tube by means of the pressure and temperature sensors.

The Pitot tube must be installed slightly sloping downwards to avoid the return of condensation that could affect the exhaust flow measurement. The pressure sensors must be installed in a region where the flow is laminar, around 4-5 diameters from the exhaust turn.

After the PEMS installation on the vehicle, some tests are needed to assess the proper connections and avoid leakages. To this purpose, the PEMS leak check and PN functionality test are performed as prescribed by the PEMS manufacturer or by legislation.

## 3.2 Onset of the test

### 3.2.1 Pre-Test

Before the RDE test, some checks must be performed to ensure the correct pollutant measurement. In particular, the pre-test procedure consists in:

- Heating the PEMS probes switching the PEMS in stand-by. This will take around 40 minutes.
- Connecting the PEMS GA to the N<sub>2</sub> and Span gas tanks.
- It is recommended to perform a long Zero before the Calibration test. This will clean the PEMS circuits leading to better measurements.
- To check if the PEMS is properly connected to the engine ECU, the car's dashboard is turned on. The PEMS should now read the engine coolant temperature.
- To check the PN functioning, with the car turned off the measurement of PN in the air should be in the order of magnitude of 10<sup>3</sup> and 10<sup>4</sup> #/m<sup>3</sup>.
- It is possible to calibrate the GA, manually or automatically, prior to the test on the Zero and Span values. A first calibration is always recommended to have more reliable measurements. The tank span concentrations must be chosen according to values of the same order of magnitude of the pollutant emissions measured during the test. To this purpose, concentrations of NO: 2500 ppmvol and CO<sub>2</sub>: 17.6 %vol have been used during the tests. A tank with a NO concentration of 960 ppmvol has

been used during a test with bad results. The calibration on such a low NO value leads to inaccuracies when higher concentrations are involved.

- The test specifications (e.g. the type of vehicle and fuel used, the span concentrations, etc.) must be set and could be saved for further tests.
- Now it is possible to start the test. An automatic calibration of the PEMS GA performing a Zero-Span-Zero starts.
- Once the tanks have been closed and disconnected by the GA, the vehicle is ready to start the RDE route with the PEMS sampling the exhaust gasses.

### 3.2.2 Post-Test

Once the RDE test has been performed, the route ended and the sampling stopped, the vehicle is brought back to the laboratory where the drift check test is performed. The test purpose is to evaluate the calibration drift at which the PEMS has been subjected during the test and is performed with a Zero-Span-Zero evaluation with the tanks connected to the GA, as during the pre-test. The measured values of Zero and Span gasses are compared to the pre-test calibration with their difference that should be compliant to the requirements of table 3.1.

In figure 3.3 the Drift check of an RDE test report is showed.

Although the absolute difference in  $\text{NO}_x$  exceeds the 5ppm criteria, the % difference is far lower than the 2% limit, thus the test is still passed. The drift check must be performed under controlled environmental conditions. The difference between the pre-test and post-test temperature of the analysers must

<b>Pollutant</b>	<b>Absolute Zero response drift</b>	<b>Absolute Span response drift</b>
CO <sub>2</sub>	≤ 2000ppm per test	≤ 2% of reading or ≤ 2000ppm per test, whichever is larger
CO	≤ 75ppm per test	≤ 2% of reading or ≤ 75ppm per test, whichever is larger
NO <sub>x</sub>	≤ 5ppm per test	≤ 2% of reading or ≤ 5ppm per test, whichever is larger
CH <sub>4</sub>	≤ 10ppm per test	≤ 2% of reading or ≤ 10ppm per test, whichever is larger
THC	≤ 10ppm per test	≤ 2% of reading or ≤ 10ppm per test, whichever is larger

Table 3.1: Drift check pollutant boundaries.

be lower than 5 °C, since the error in the measurements increases with the temperature difference. Since the failure in the measurement of just one of the zero or pollutants during the check means the failure of the entire RDE test, it is not uncommon to start the drift check for delta temperatures around 2.5 °C.

### 3.3 Emissions determination

#### 3.3.1 Corrections

Although the measurements are made directly on engine exhaust, some corrections are still needed:

- If the emissions are measured on dry basis, the conversion to wet basis is needed according to the equation 3.4.

$$c_{wet} = k_w \cdot c_{dry} \quad (3.4)$$

## Drift Check Report

Test		Vehicle		Device	
Test ID	:	Vehicle Name	:	Cell Name	: OBS-ONE
Test Date	:	Vehicle Category	:	Cell Description	:
Test Start	:	Vehicle Class	:		
Test End	:	Vehicle Type	: ICE		
Driver	:	Fuel Type	: Diesel		
Comment	:	Description	:		

Drift Check Result					
Zero Drift					
	Unit	Pre	Post	Abs. Diff.	Criteria
CO	ppm	-2.81	1.05	3.86	<= 75
CO2	ppm	67.11	73.16	6.05	<= 2000
NOx	ppm	0.90	-0.12	1.02	<= 5
NO	ppm	0.10	-0.01	0.11	—
THC	ppmC	0.00	0.00	0.00	<= 10
CH4	ppmC	0.00	0.00	0.00	<= 10

Span Drift								
	Unit	Pre	Post	Abs. Diff.	Criteria	Abs. %RS	Criteria	Overall
CO	ppm	19933.75	19983.50	49.75	<= 75	0.25 %	<= 2 %	Pass
CO2	ppm	176878.00	177170.30	292.30	<= 2000	0.17 %	<= 2 %	Pass
NOx	ppm	2505.32	2497.32	7.99	<= 5	0.32 %	<= 2 %	Pass
NO	ppm	2504.32	2490.83	13.49	—	0.54 %	—	—
THC	ppmC	0.00	0.00	0.00	<= 10	—	<= 2 %	Pass
CH4	ppmC	0.00	0.00	0.00	<= 10	—	<= 2 %	Pass

Judge      Pass : Green      Fail : Red

Figure 3.3: Drift check report.

Defining  $c_{wet}$  as the wet concentration of a pollutant in ppm or per cent volume,  $c_{dry}$  as the dry concentration of a pollutant in ppm or per cent volume, and  $k_w$  as the dry-wet correction factor.

- The corrections for ambient temperature and humidity are not needed.
- The negative results are set to zero.
- Corrective factors for extended environmental conditions are applied if

needed.

- The emissions and exhaust mass flow rate are time shifted and corrected according to their transformation time.
- The ECU data are time-aligned with the PEMS emission data.

### 3.3.2 Instantaneous emissions

The PEMS measures the instantaneous concentration of the gaseous pollutant and evaluates the mass of the exhaust component based on the exhaust mass flow rate and the density ratio of the exhaust component according to the equation 3.5.

$$m_{gas,i} = u_{gas} \cdot c_{gas,i} \cdot q_{mew,i} \quad (3.5)$$

Where  $m_{gas,i}$  is the mass of the exhaust component 'gas' [g/s],  $u_{gas}$  is the ratio of the density of the exhaust component 'gas' and the overall density of the exhaust,  $c_{gas,i}$  is the measured concentration of the exhaust component 'gas' in the exhaust [ppm],  $q_{mew,i}$  is the measured exhaust mass flow rate [kg/s],  $gas$  is the respective component, and  $i$  is the number of the measurement.

In a similar way, the instantaneous particle emissions are determined by multiplying the particle number concentration with the instantaneous mass flow rate, according to equation 3.6.

$$PN,i = \frac{c_{PN,i} \cdot q_{mew,i}}{\rho_e} \quad (3.6)$$

Where  $PN,i$  is the particle number flux [particles/s],  $c_{PN,i}$  is the measured

particle number concentration [ $\#/m^3$ ] normalized at 0 °C,  $q_{mew,i}$  is the measured exhaust flow rate [kg/s], and  $\rho_e$  is the density of the exhaust gas [kg/m<sup>3</sup>] at 0 °C.

The values of exhaust density and density ratio are expressed according to the type of fuel selected during the test parameter definition in section 3.2.1, and are reported in figure 3.4.

Fuel	$\rho_e$ [kg/m <sup>3</sup> ]	Component or pollutant i					
		NO <sub>x</sub>	CO	HC	CO <sub>2</sub>	O <sub>2</sub>	CH <sub>4</sub>
		$\rho_{gas}$ [kg/m <sup>3</sup> ]					
		2,053	1,250	( <sup>1</sup> )	1,9636	1,4277	0,716
$u_{gas}$ ( <sup>2</sup> ), ( <sup>6</sup> )							
Diesel (B7)	1,2943	0,001586	0,000966	0,000482	0,001517	0,001103	0,000553
Ethanol (ED95)	1,2768	0,001609	0,000980	0,000780	0,001539	0,001119	0,000561
CNG ( <sup>3</sup> )	1,2661	0,001621	0,000987	0,000528 ( <sup>4</sup> )	0,001551	0,001128	0,000565
Propane	1,2805	0,001603	0,000976	0,000512	0,001533	0,001115	0,000559
Butane	1,2832	0,001600	0,000974	0,000505	0,001530	0,001113	0,000558
LPG ( <sup>5</sup> )	1,2811	0,001602	0,000976	0,000510	0,001533	0,001115	0,000559
Petrol (E10)	1,2931	0,001587	0,000966	0,000499	0,001518	0,001104	0,000553
Ethanol (E85)	1,2797	0,001604	0,000977	0,000730	0,001534	0,001116	0,000559

(<sup>1</sup>) depending on fuel  
(<sup>2</sup>) at  $\lambda = 2$ , dry air, 273 K, 101.3 kPa  
(<sup>3</sup>)  $u$  values accurate within 0,2 % for mass composition of: C=66-76 %; H=22-25 %; N=0-12 %  
(<sup>4</sup>) NMHC on the basis of CH<sub>2,93</sub> (for THC the  $u_{gas}$  coefficient of CH<sub>4</sub> shall be used)  
(<sup>5</sup>)  $u$  accurate within 0,2 % for mass composition of: C<sub>3</sub>=70-90 %; C<sub>4</sub>=10-30 %  
(<sup>6</sup>)  $u_{gas}$  is a unitless parameter; the  $u_{gas}$  values include unit conversions to ensure that the instantaneous emissions are obtained in the specified physical unit, i.e., g/s

Figure 3.4: Raw exhaust gas values.

### 3.3.3 Calculation of the final emissions

The distance-specific mass of CO<sub>2</sub> emitted for ICE Vehicles, Not Off-Vehicle Chargeable Hybrid Electric Vehicles (NOVC-HEV), and Off-Vehicle Charge-

When:	Then the Result evaluation factor $RF_k$ is:	Where:
$r_k \leq RF_{L1}$	$RF_k = 1$	
$RF_{L1} < r_k \leq RF_{L2}$	$RF_k = a_1 r_k + b_1$	$a_1 = \frac{RF_{L2} - 1}{[RF_{L2}(RF_{L1} - RF_{L2})]}$ $b_1 = 1 - a_1 RF_{L1}$
$r_k > RF_{L2}$	$RF_k = \frac{1}{r_k}$	

Figure 3.5: RF evaluation.

able Hybrid Electric Vehicles (OVC-HEV) during the RDE cycle must be multiplied by a Result Evaluation Factor (RF) according to the equation 3.7.

$$M_{RDE,k} = m_{RDE,k} \cdot RF_k \quad (3.7)$$

Where  $M_{RDE,k}$  is the final RDE distance-specific mass of gaseous pollutants [mg/km] or particle number [# / km],  $m_{RDE,k}$  is the distance-specific mass of gaseous pollutants [mg/km] or particle number [# / km] emissions, emitted over the complete RDE trip and prior to any correction.

Defined the limit values  $RF_{L1} = 1.30$  and  $RF_{L2} = 1.50$ , the RF factor is calculated according to the figure 3.5, introducing the  $r_k$  as the ratio between the distance specific CO<sub>2</sub> emissions measured during the RDE and WLTP. If an OVC-HEV is considered, the emissions during the WLTP must be the one using the Charge Sustaining mode. In this case, the  $r_k$  is defined as in equation 3.8.

$$r_k = \frac{M_{CO_2,RDE,k}}{M_{CO_2,WLTP,k-CS,t}} \cdot \frac{0.85}{IC_k} \quad (3.8)$$

Defining the value  $IC_k$  as the ratio of the distance driven with the combustion engine divided by the total trip distance in equation 3.9.

$$IC_k = \frac{d_{ICE,k}}{d_{ICE,k} + d_{EV,k}} \quad (3.9)$$

Where  $M_{CO_2,RDE,k}$  is the distance-specific mass of CO<sub>2</sub> [g/km], emitted over the RDE trip, and  $M_{CO_2,WLTP,k}$  is the distance-specific mass of CO<sub>2</sub> [g/km], emitted over the WLTP trip, as to consider the usage of the ICE during both tests.

## 3.4 Verification of the trip dynamics

### 3.4.1 Verification of the dynamics through the MAW

To evaluate whether the trip is valid for RDE purposes, the test is divided into sub-sections called windows. Each window is defined so as to match always the same CO<sub>2</sub> reference mass. The CO<sub>2</sub> mass is determined by integration of the instantaneous emissions. Once the window is defined, a new window starts according after a  $\Delta t$  corresponding to the data sampling frequency which is, in our case, 1Hz. The duration of a  $j^{th}$  window is determined by the equation 3.10.

$$M_{CO_2}(t_{2,j}) - M_{CO_2}(t_{1,j}) \geq M_{CO_2,ref} \quad (3.10)$$

Defined  $M_{CO_2,ref}$  as half of the CO<sub>2</sub> mass emitted by the vehicle over the WLTP test. Also,  $t_{2,j}$  is selected according to the criteria expressed by equation 3.11.

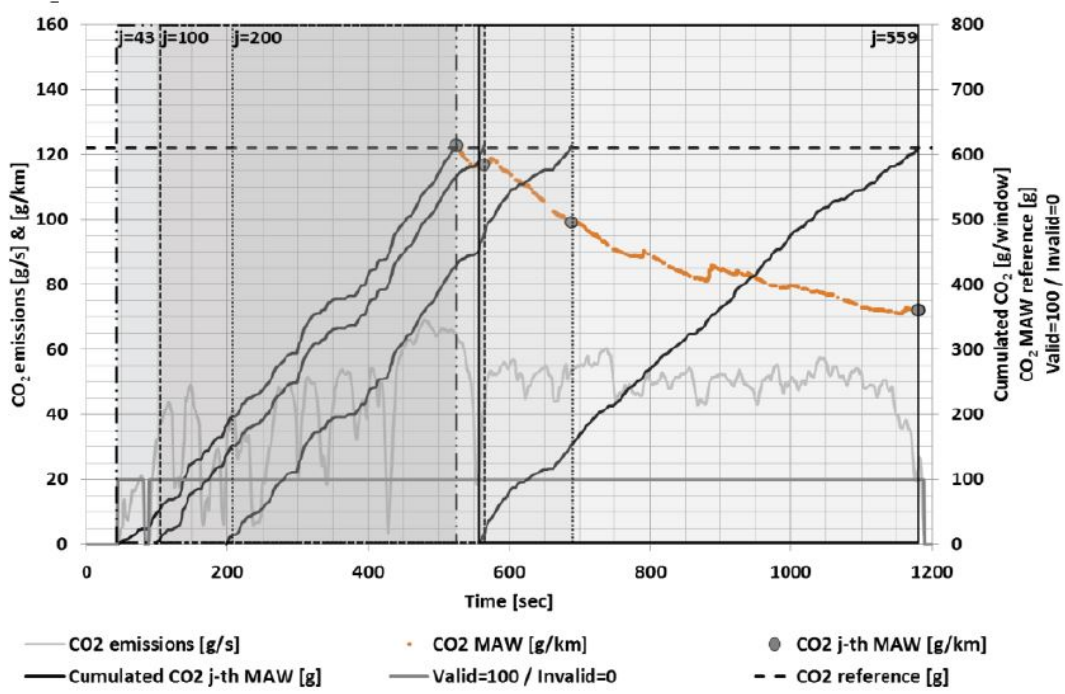


Figure 3.6: Window calculation example [5].

$$M_{CO_2}(t_{2,j} - \Delta t) - M_{CO_2}(t_{1,j}) < M_{CO_2,ref} < M_{CO_2}(t_{2,j}) - M_{CO_2}(t_{1,j}) \quad (3.11)$$

Each window is averaged and plotted as a point on the 'vehicle CO<sub>2</sub> characteristic curve', which is the dynamic reference condition, defined as a vehicle CO<sub>2</sub> emissions vs average speed measured during WLTP. An example of the window calculation is presented in figure 3.6 [5].

The curve is defined by the three points P1, P2 and P3 defined as follows:

- Point 1:

$$v_{P1} = 18.882 \text{ km/h.}$$

$$M_{CO_2,d,P1} = \text{vehicle CO}_2 \text{ emissions over the low speed phase of the WLTP}$$

cycle [g/km]

- Point 2:

$$v_{P2} = 56.664 \text{ km/h.}$$

$M_{CO_2,d,P2}$  = vehicle CO<sub>2</sub> emissions over the high speed phase of the WLTP cycle [g/km]

- Point 3:

$$v_{P3} = 91.997 \text{ km/h.}$$

$M_{CO_2,d,P3}$  = vehicle CO<sub>2</sub> emissions over the extra high speed phase of the WLTP cycle [g/km]

The speeds are obtained as average speeds of the low, high and extra high phases of the WLTP cycle. The characteristic curve is obtained using two linear sections, P1-P2 and P2-P3, with the last one limited to 145km/h on the vehicle speed axis. Defined the curve, the windows calculated can be classified by average vehicle speed in:

- Urban windows: with an average speed lower than 45 km/h;
- Rural windows: with an average speed greater than or equal to 45 km/h and lower than 80 km/h;
- Motorway windows: with an average speed greater than or equal to 80 km/h and lower than 145 km/h;

The characteristic curve presents an upper tolerance of 45% for urban driving and 40% for rural and motorway, and a lower tolerance for ICE and NOVC-HEV vehicles of 25% (OVC-HEV vehicles' tolerance is 100%). The test is valid

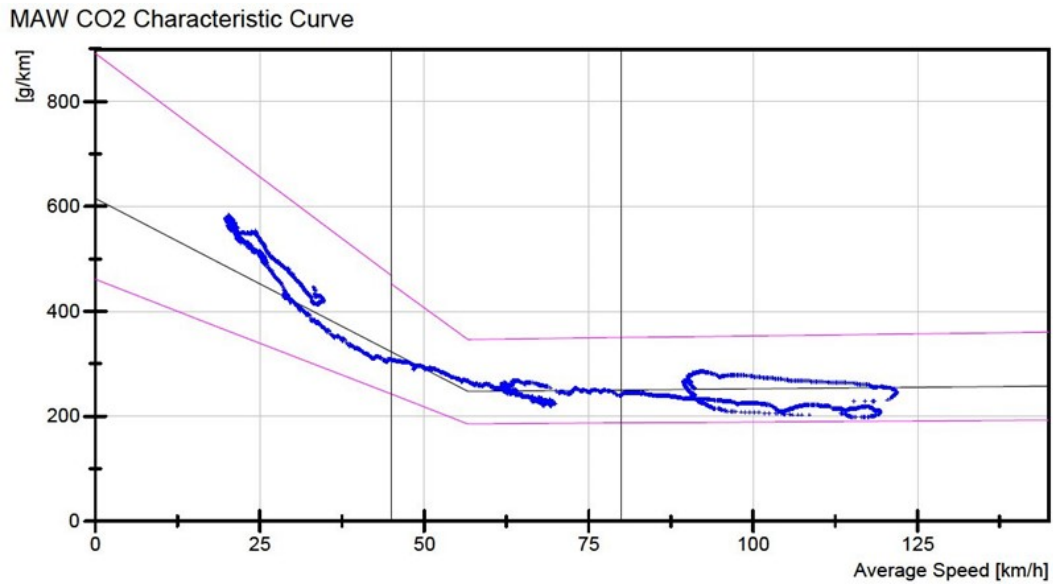


Figure 3.7: MAW CO<sub>2</sub> characteristic curve.

when it comprises at least 50% of the urban, rural and motorway windows that are within the tolerances defined. An example is presented in figure 3.7, in this case the 100% of windows are within the tolerances.

### 3.4.2 Verification of the dynamics through the calculation of $v_{a,pos}$ and RPA

This procedure verifies the trip dynamics by determining the excess or absence of dynamics during the three test's phases. The two dynamic parameters to be evaluated are:

- $v_{a,pos}$  defined as the vehicle speed per positive acceleration greater than  $0.1 \frac{m}{s^2}$ .
- Relative Positive Acceleration (RPA).

Both those parameters are evaluated with a frequency of 1Hz. The datasets shall be divided depending on the vehicle speed into urban ( $v_{inst} \leq 60km/h$ ), rural ( $60km/h < v_{inst} \leq 90km/h$ ) and motorway bins ( $v_{inst} > 90km/h$ ). The values of  $v_{a,pos}$  and RPA shall fulfil certain criteria to have a valid test. In the figure 3.8 is possible to easily evaluate if these criteria are fulfilled: the cycle is valid if the  $v_{a,pos}$  points are below its limit curve and the RPA points are above its limit curve. If the  $v_{a,pos}$  is above its limit curve means that the driver has been too aggressive during the driving, on the contrary the RPA below the limit curve suggests a too soft driving style.

### 3.5 Data analysis and validation

All the data needed for the vehicle RDE compliance are obtained through the report generated by the Horiba software. In the following, some of the RDE reports of the tests performed are represented.

In the first cycle, in figure 3.9, the route trip composition is RDE compliant although the small motorway section, interrupted by urban and rural parts due to the traffic jam.

Nevertheless, the test is still not acceptable due to the motorway valid window ratio. The MAW statistics are represented in figure 3.10.

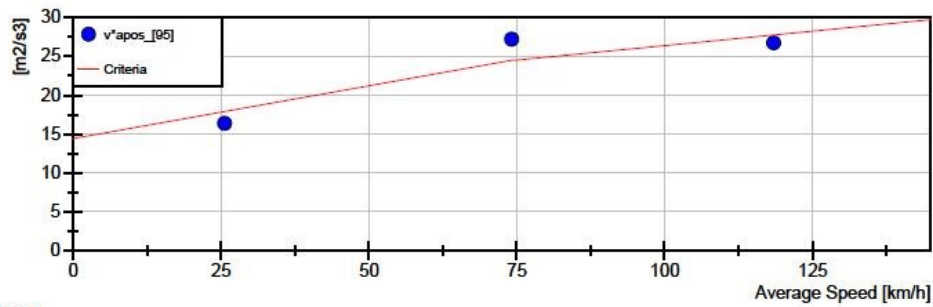
Analysing the GPS data from the PEMS acquisitions in figure 3.11, it is possible to notice that in the motorway part the road slope is negative, thus the acceleration needed to maintain the vehicle at the motorway speed is not sufficient to generate the CO<sub>2</sub> needed for the windows validation. This problem could be solved changing the motorway route, but it is just one of the many

Dynamics

	Unit	Urban	Rural	Motorway
Data Count	#	4255	1410	1069
Positive Data Count	#	1499	382	231
Criteria	#	>= 100	>= 100	>= 100
Average Speed	km/h	25.59	74.13	118.43
$v^*_{apos}_{[95]}$	m2/s3	16.390	27.246	26.773
Criteria	m2/s3	<= 17.921	<= 24.521	<= 27.754
RPA	m/s2	0.259	0.128	0.069
Criteria	m/s2	>= 0.135	>= 0.057	>= 0.025

Judge Pass : Green Fail : Red

$v^*_{apos}_{[95]}$



RPA

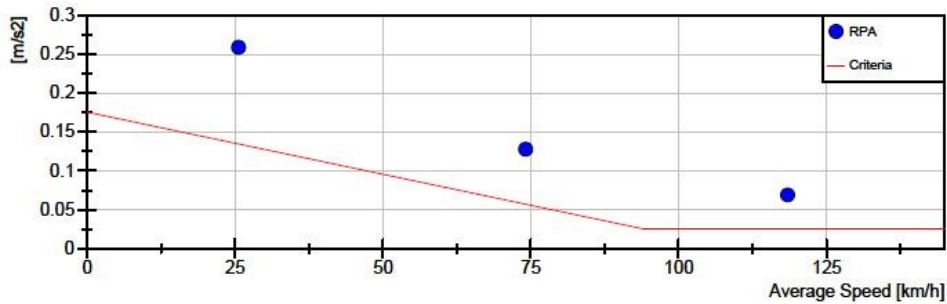


Figure 3.8: Trip dynamics verification in a report.

problems related to the trip definition.

In this second cycle, defined by the figure 3.12, the trip definition is RDE compliant, the CO<sub>2</sub> windows are valid, and the drift checks are inside the tolerances. What does make the test not acceptable is the dynamic in figure 3.13.

According to section 3.4.2 the value of the  $v_{a,pos}$  should be below the limit curve to be RDE compliant. The values above the criteria define a driving

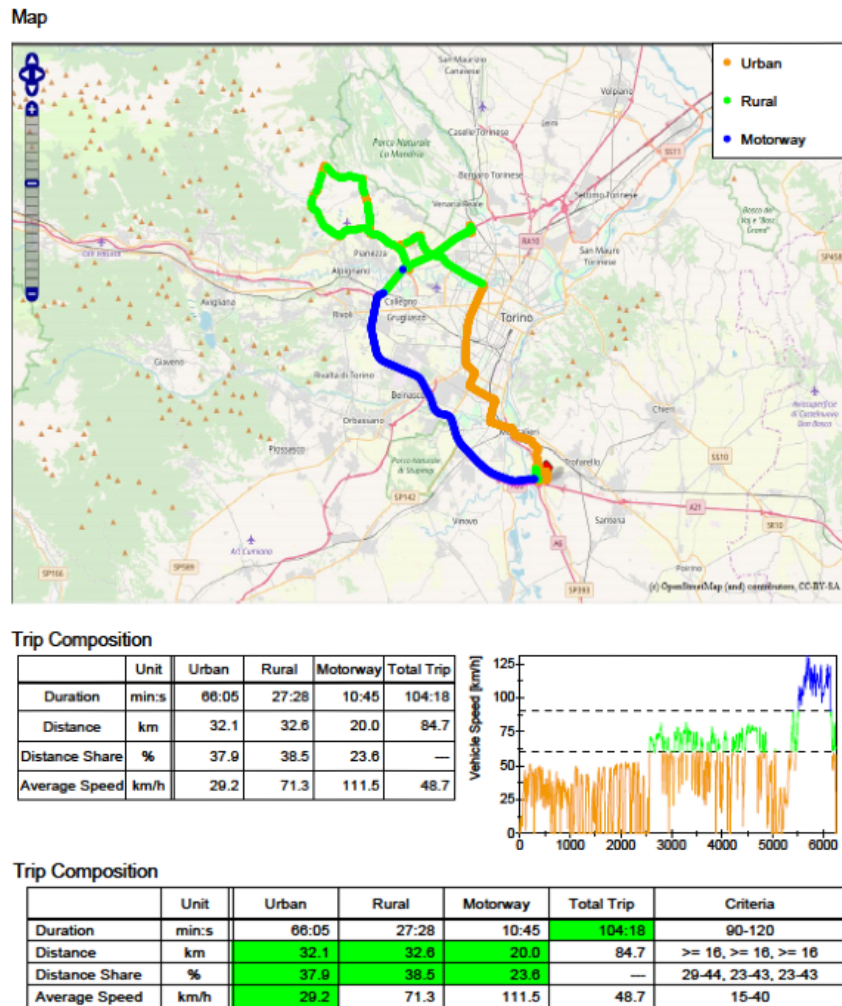


Figure 3.9: Trip composition of the first RDE test.

style that is way too aggressive, obviously affecting the emissions. Comparing the  $\text{NO}_x$  emissions of this test with the ones of another test performed with the same vehicle, same route and a “softer” driving style RDE compliant in figure 3.14, it is possible to notice a difference that is quite representative of the importance of the dynamics during the test assessment.

## CHAPTER 3. ON-ROAD RDE TESTING

### MAW Statistics

	Unit	Urban	Rural	Motorway	Total	Over
Upper Tol1(H)	#	0	0	0	0	0
Inside Tol1	#	1204	3113	225	4542	0
Lower Tol1(L)	#	0	131	237	368	0
Total	#	1204	3244	462	4910	0
Valid Window Ratio	%	100.0	98.0	48.7	92.5	0.0
Criteria	%	>= 50	>= 50	>= 50	---	---

Judge    Pass : Green    Fail : Red

### Tolerance

	Unit	Urban	Rural	Motorway
Tol1(H)	%	45	40	40
Tol1(L)	%	25	25	25

### MAW CO2 Characteristic Curve

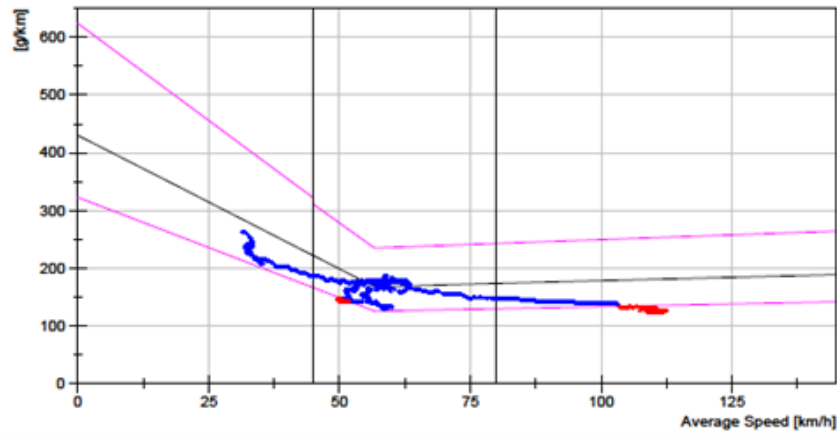


Figure 3.10: MAW statistics of the first RDE test.

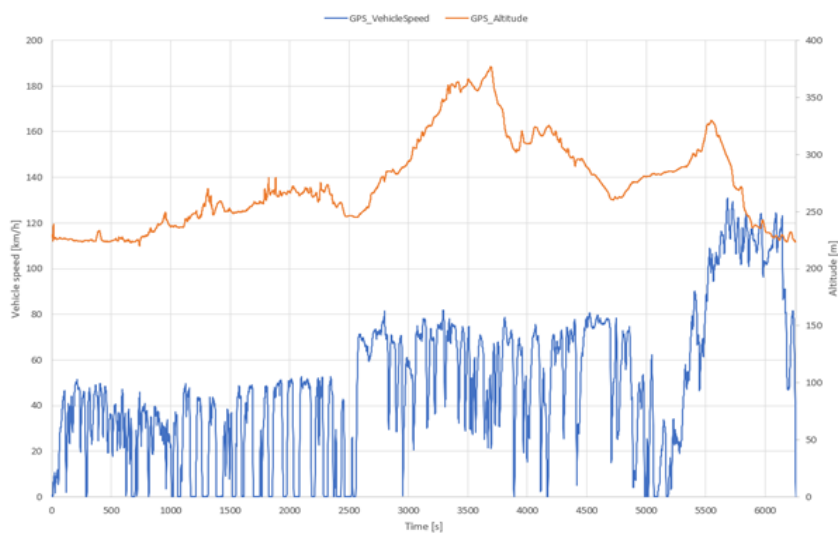


Figure 3.11: GPS altitude and vehicle speed over the first RDE cycle.

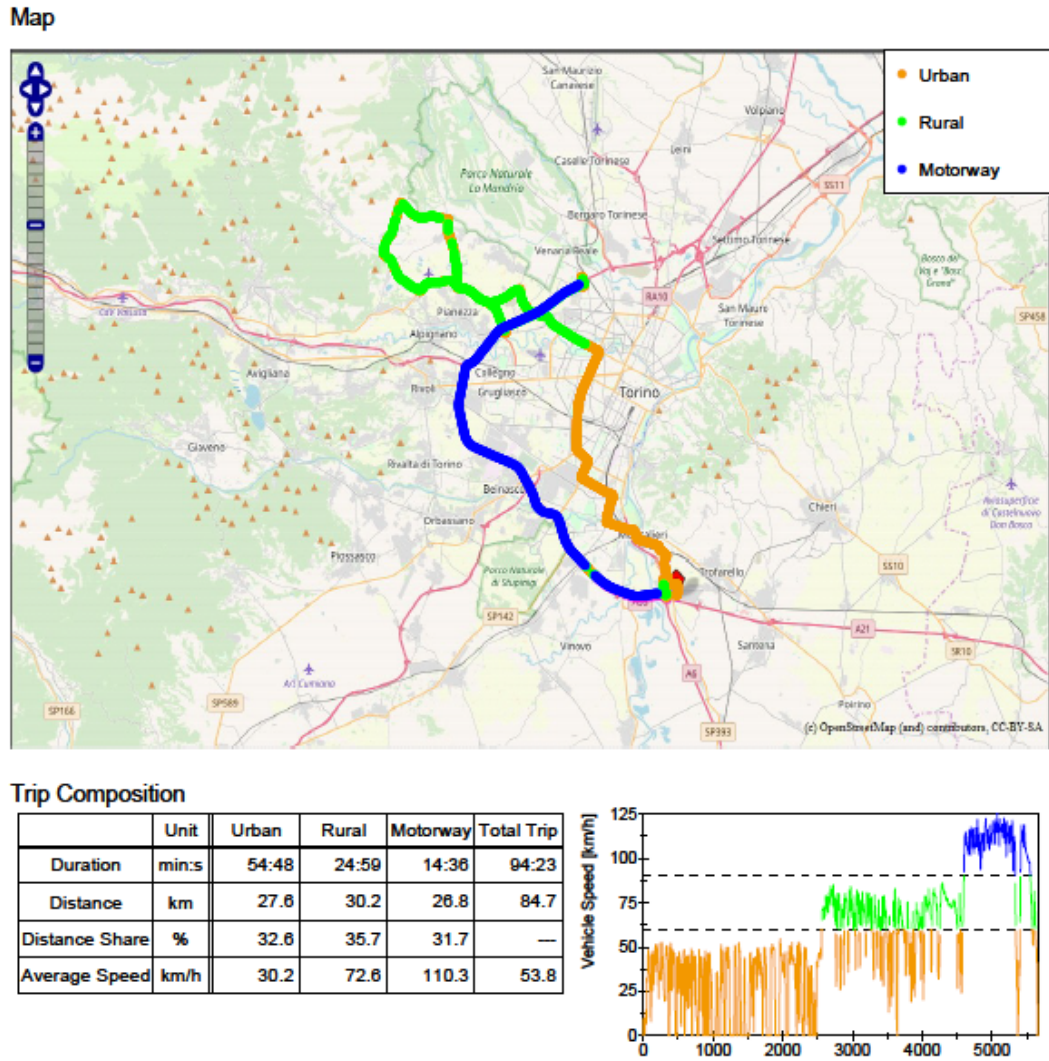


Figure 3.12: Trip composition of the second RDE test.

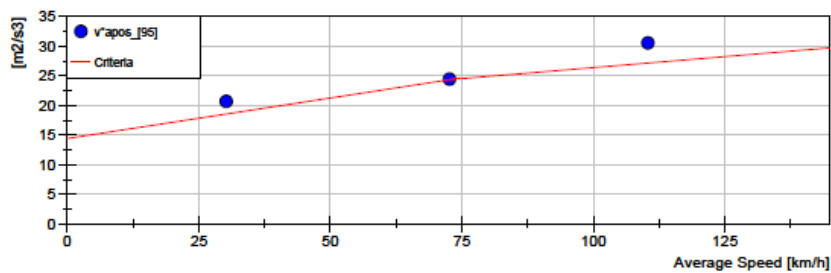
## CHAPTER 3. ON-ROAD RDE TESTING

### Dynamics

	Unit	Urban	Rural	Motorway
Data Count	#	3288	1499	876
Positive Data Count	#	971	342	216
Criteria	#	>= 100	>= 100	>= 100
Average Speed	km/h	30.19	72.64	110.34
$v^{\ast}apos_{[95]}$	m2/s3	20.694	24.434	30.599
Criteria	m2/s3	<= 18.546	<= 24.319	<= 27.153
RPA	m/s2	0.275	0.131	0.127
Criteria	m/s2	>= 0.127	>= 0.059	>= 0.025

Judge    Pass : Green    Fail : Red

### $v^{\ast}apos_{[95]}$



### RPA

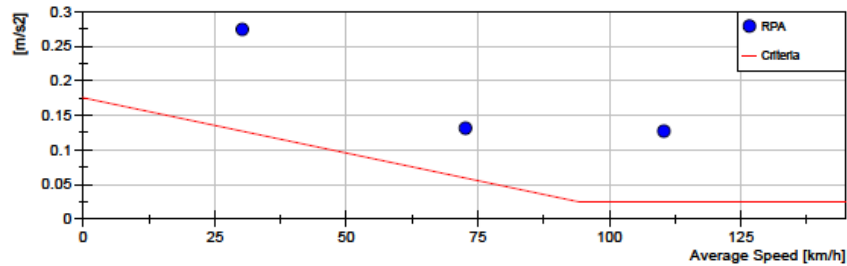


Figure 3.13: Dynamics of the second RDE test.

### Final Emission

	Unit	Final Emission		NTE Pollutant
		Urban	Total Trip	
CO	mg/km	518.979	253.669	---
CO2	g/km	251.623	179.685	---
NOx	mg/km	45.095	17.927	114.40

### Final Emission

	Unit	Final Emission		NTE Pollutant
		Urban	Total Trip	
CO	mg/km	304.750	153.918	---
CO2	g/km	244.569	174.453	---
NOx	mg/km	23.977	10.216	114.40

Figure 3.14: Final emissions comparison between tests with different dynamics. In the upper table a more aggressive driving style is adopted.

# Chapter 4

## Test cycle simulation

### 4.1 Introduction to the simulation advantages and limits

Although the prototype testing still plays a major role in the vehicle development, in the last years the numerical simulation has received much attention. Through the implementation of vehicle models that reproduce their behaviour, carmakers can save a huge amount of time and money. Moreover, the vehicles can be deeply investigated without any physical risk. The application of simulation covers the most various fields in the automotive industries, starting from the emission control systems efficiency [18], to the simulation of the vehicle's shock absorber dynamics [19]. Although the computer simulation is known to be a powerful tool, reducing the need of a prototype to validate a design, it implies limitations making the on-vehicle testing still needed. A major problem could be related, for example, to the high model calibration effort, or the accuracy of the model due to nonlinear components.

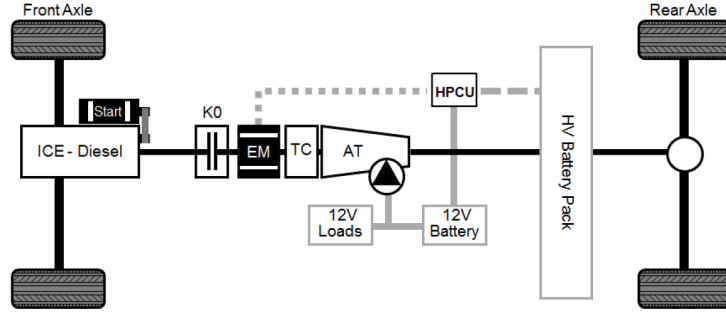


Figure 4.1: Vehicle's powertrain scheme [6].

To investigate on the possibility of adopting the numerical simulation for the CO<sub>2</sub> prediction, a vehicle among the fleet tested in FEV Italia has been considered and modelled. The model has been calibrated over experimental NEDC and WLTP procedures, prior to the RDE simulation. The results obtained have been compared to the experimental values obtained through a measuring campaign.

## 4.2 Model setup

The vehicle considered for the simulation is the same of [6]: a P2 Diesel Plug-In Hybrid Electric Vehicle featuring a permanent magnet synchronous Electric Motor (EM) mounted downstream the ICE and coupled with an additional clutch allowing the disengagement of ICE and EM during the full electric mode. The powertrain scheme and specifications are defined in figures 4.1 and 4.2.

The software used for the model development is GT-Suite, coupled with a Simulink model for the hybrid mode control logic. The starting model is obtained through reverse engineering of the vehicle's hybrid control logic using

Engine (ICE)	
Engine Type	In-line 4 cyl. Turbo Diesel
Displacement	1950 cc
Max Power / Max Torque	143kW @3800rpm / 400Nm @1600-2800 rpm
Compression Ratio	15.5:1
Transmission	
6° BTDC @ 0.15 mm lift	
Type	9 –AT w/ Torque Converter
Speed Ratios	I 5.36      IV 1.64      VII 0.87
	II 3.25      V 1.22      VIII 0.72
	III 2.26      VI 1.00      IX 0.61
Reverse – Final Drive	- 4.93      2.65
Vehicle	
6° BTDC @ 0.15 mm lift	
Curb Weight	2060 kg
Configuration	Rear Wheel Drive (RWD)
Electric Motor (EM)	
Type	PM Synchronous motor
Max Power / Max Torque	90 kW / 440 Nm @1750rpm
Max Speed	6000 rpm
High Voltage Battery	
Type	Lithium- NMC
Rated Voltage	365V
Capacity	13.5kWh / 37 Ah
Cooling System	Water Cooled

Figure 4.2: Vehicle’s specifications [6].

the experimental data of paper [6], allowing the simulation of NEDC and WLTP homologation cycles with a vehicle behaviour that is very much representative of the actual vehicle’s one. To reduce the computational time, the engine is map-based by means of experimental maps concerning the engine efficiency, the power loss, and the fuel consumption. For what concerns the EM’s behaviour, again a map-based model is implemented considering the motor’s torque, efficiency, and rotor’s inertia. The Simulink control logic defines whether to go in Hybrid mode or Electric mode depending on the driver’s demand. The model layout is the one in figure 4.5.

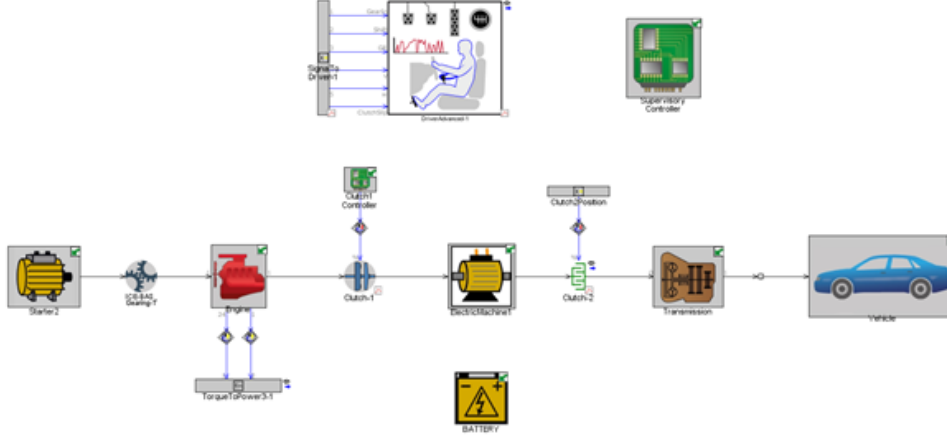


Figure 4.3: Model layout.

The RL are the one calculated for the NEDC and WLTP onset, thus obtained experimentally through coast-down tests. The type of analysis implemented is of the "quasi-static" approach. The ICE rotational speed is obtained through kinematic relationships starting from the vehicle speed and involving the transmission ratios, but the torque needed by the vehicle to follow the speed trace is determined by the driver block, which is defined as a PID controller, once the longitudinal vehicle dynamics equation are solved according to figure 4.4 [7].

The vehicle equilibrium equation is obtained considering the force needed to overcome the rolling  $F_{roll}$ , aerodynamic  $F_{aero}$ , and gradient  $F_{grade}$  resistance forces in equation 4.1.

$$F_{tract} = F_{pwt} - F_{brakes} = F_{inertia} + F_{grade} + F_{roll} + F_{aero} \quad (4.1)$$

The ICE is characterised by a fuel consumption map returning an instantaneous fuel consumption rate as function of the torque and engine angular

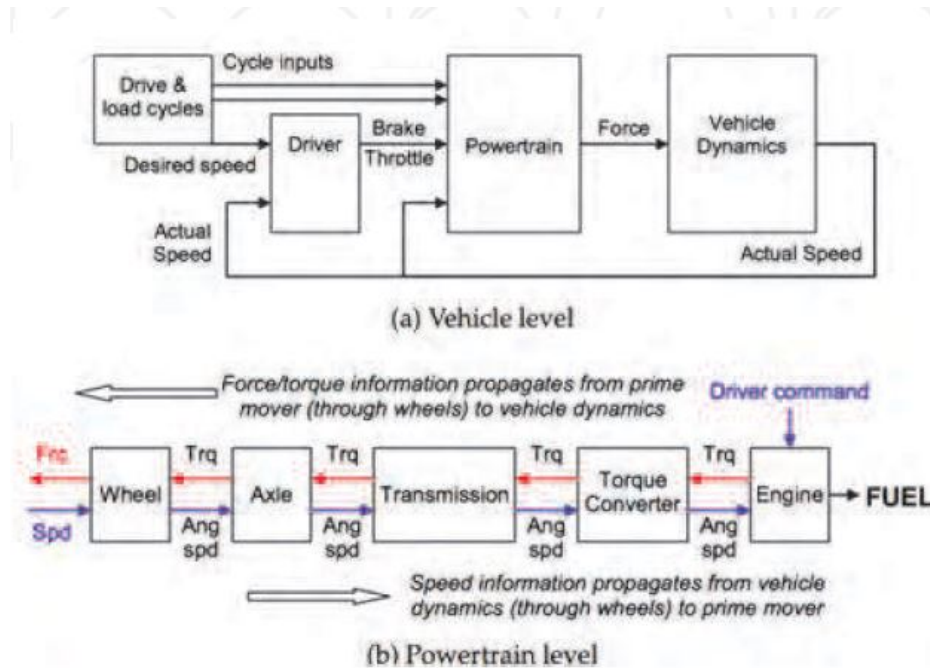


Figure 4.4: Information flow in a quasi-static powertrain model [7].

speed. This type of simulation allows to perform fuel consumption evaluations with a relatively low computational time.

### 4.3 Controls implemented

The above model is capable to run the NEDC and WLTP cycles following the real vehicle's hybrid control logic. Although the important result and the high reverse engineering effort needed to capture the logic behind the ECU mode definition, the aim of this work is to validate the model on already taken experimental cycles, thus some changes are needed to let the model reproduce cycles' emissions. To this purpose, different control strategies have been implemented focusing on 1 degree of freedom models. The idea behind all the models is to impose the torque profile related to the ICE or the EM

and to obtain the other as difference between the torque needed by the driver and the one imposed, allowing one of the two propulsion systems to satisfy the torque demand since not bounded to the experimental profile. Another idea is to calculate an experimental torque split ratio to be multiplied by the driver torque demand, obtaining both the torque profiles as function of the driver torque demand. Anyway, all the models have been implemented and evaluated starting from an experimental NEDC cycle. Since the starting model is not implemented to have a torque imposition, but evaluates the torque split needed by means of a Simulink control logic telling the ECU whether to switch on/off the engine and go hybrid or electrical mode, different controls have been applied bypassing the Simulink logic. The main ones are related to:

- The torque profile impositions.
- The engine switch profile.
- The operation MODE bypass.

## 4.4 Cycles simulation

### 4.4.1 NEDC simulation

Generally, in this model the NEDC simulation the driver torque demand is higher compared to the experimental total torque provided by the powertrain system. Since one of the two torque profiles, or both in the case of the torque split ratio imposition, depends upon the driver torque demand, this discrepancy affects the definition of the torque profiles obtained. In figure 4.5 the evaluation of the total torque required is showed, zooming on the final part

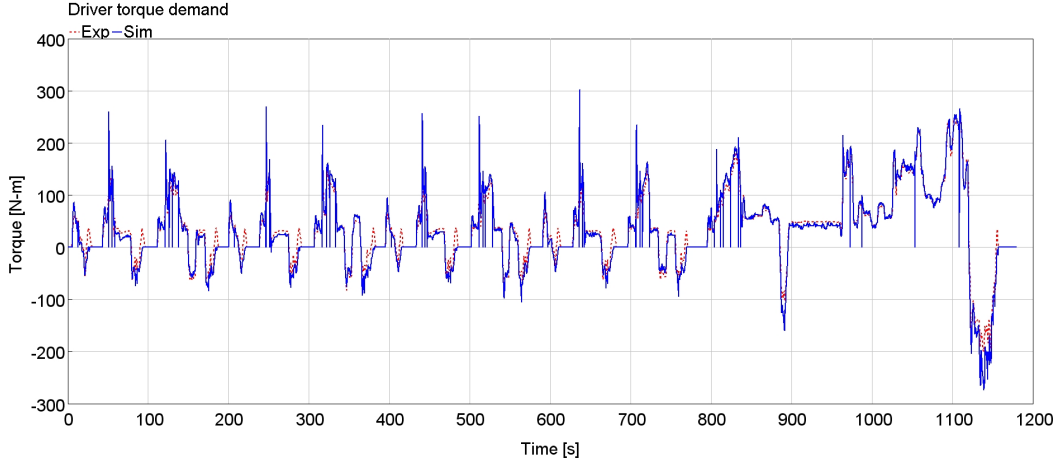


Figure 4.5: NEDC Driver Torque Demand.

of the homologation cycle including an ECE and the EUDC part. The trend of the driver torque demand is common to all the NEDC models since not dependent on the type of control implemented.

The torque profiles impositions bypass the Simulink control logic and directly actuate the ICE and EM through the signal receivers, but to be effective the engine switch profile and mode, when needed, must be bypassed as well. Furthermore, the experimental data profiles needed to be filtered to avoid spikes related to measuring issues. The switch profile is obtained experimentally starting from the ECU fuel consumption profile, imposing the ICE turned on for positive values of the fuel consumption. To this purpose a simple MATLAB code is implemented, having as result a binary profile to be imposed to the ICE simulation block for the NEDC cycle.

Hereafter, the three types of model implemented for the NEDC reproduction are presented, with the results reported in table 4.1.

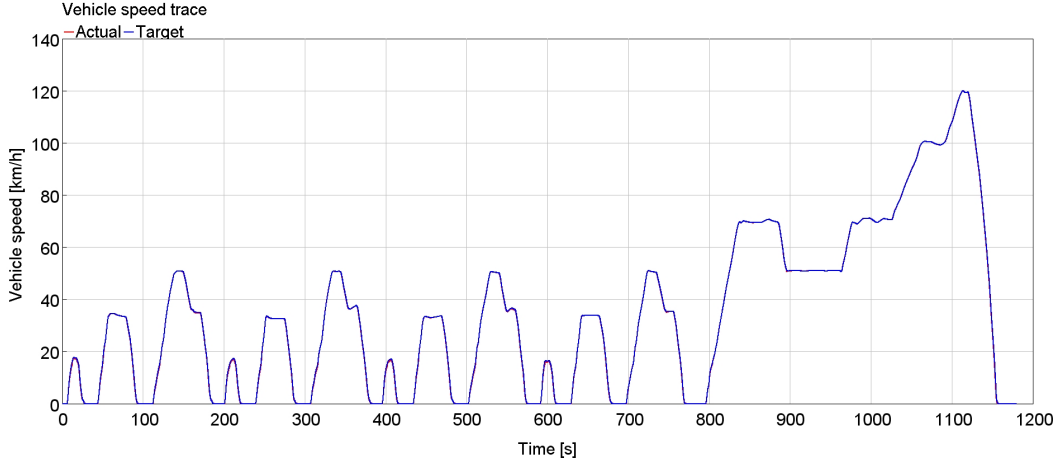


Figure 4.6: NEDC speed trace profile of the torque split imposition model.

**Torque Split Profile Imposition Model:** Imposing the torque split, the ratio between the torque provided by the EM and ICE is defined starting from the experimental profiles, thus avoiding lack of torque demanded by the driver and allowing the driver to properly follow the speed trace. As advantage, it is possible for the powertrain to provide the total amount of torque needed by the driver preventing overload of one propulsion system with respect to the other or torque gaps during all the operative modes. As drawback, the whole profiles are shifted upwards due to the higher torque demand of the driver, leading to a greater usage of the ICE that is traduced into higher consumptions compared to the experimental values. Nevertheless, the speed trace in figure 4.6 is perfectly followed by the driver.

The torque profiles are evaluated in equations 4.2 and 4.3.

$$Torque_{ICE,Sim} = \frac{Torque_{ICE,Exp}}{Torque_{Total,Exp}} \cdot Torque_{DriverDemand,Sim} \quad (4.2)$$

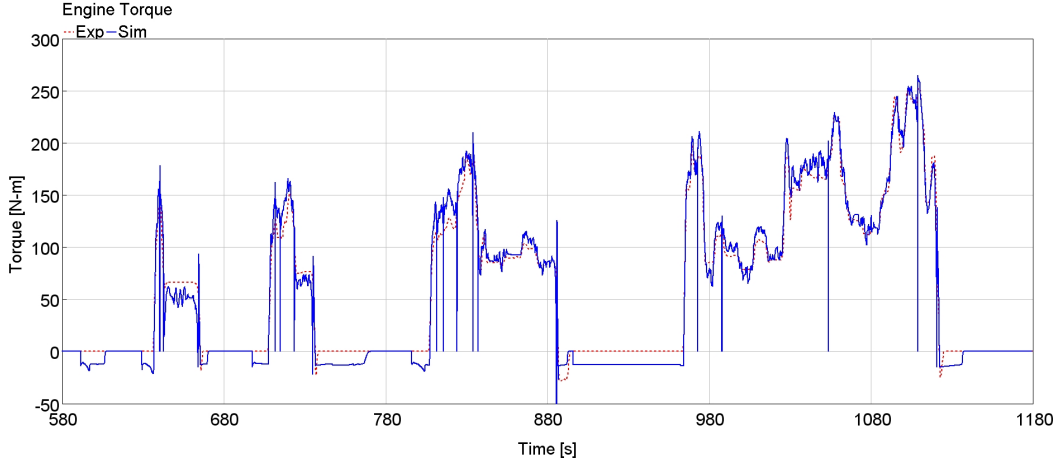


Figure 4.7: NEDC Engine torque profile of the torque split imposition model.

$$Torque_{EM,Sim} = Torque_{DriverDemand,Sim} - Torque_{ICE,Sim} \quad (4.3)$$

And their plots are showed in figures 4.7 and 4.8.

It is interesting to evaluate the trend of the battery State Of Charge (SOC) too. The simulated SOC is compared to the experimental one obtained by dashboard reading. This comparison is made in figure 4.9.

As previously said, the higher driver torque demand compared to the experimental values leads to a more intense use of the powertrain system, with the torque profiles that overestimate the experimental ones. The simulated cumulative fuel consumption in figure 4.10 shows a good match with the experimental values until an extended use of the ICE in the EUDC part.

Although the good accuracy of the model on this cycle, it will not be further implemented due to an inevitable increase of the error related to a greater usage of the ICE in the other homologation cycles.

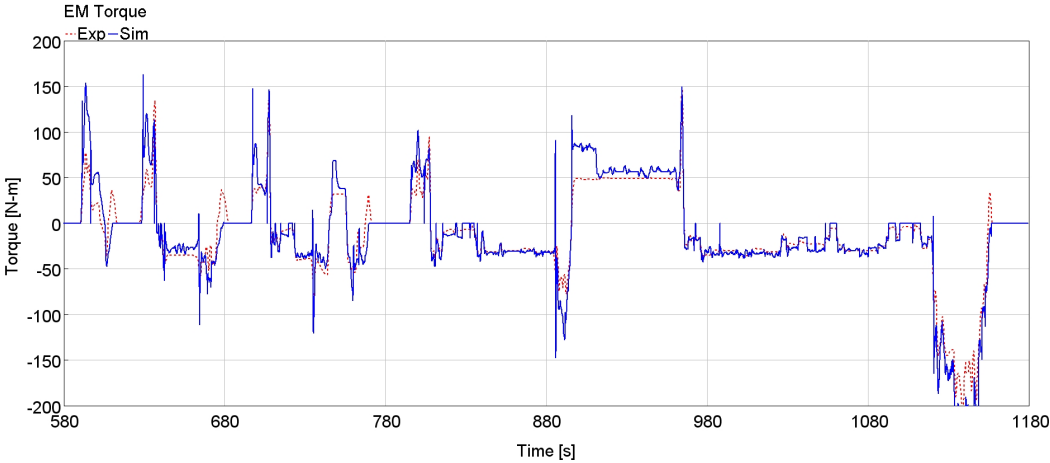


Figure 4.8: NEDC EM torque profile of the torque split imposition model.

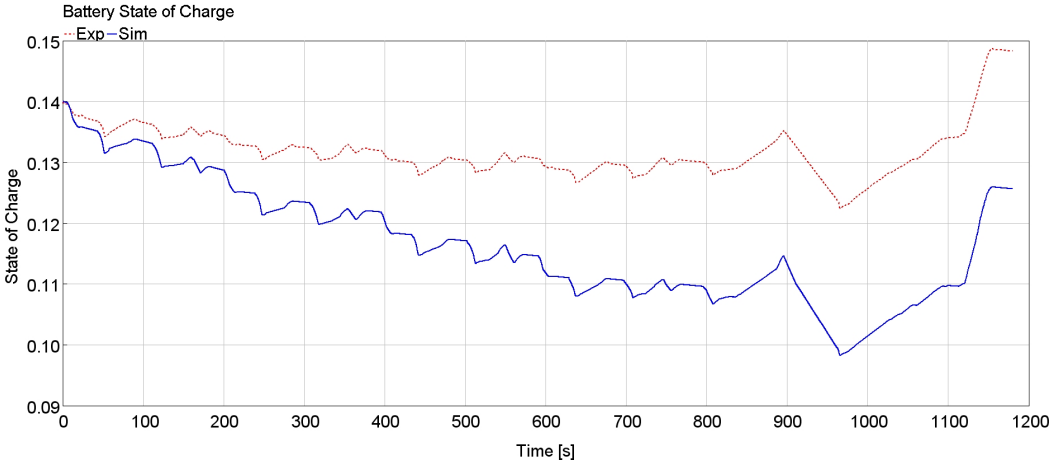


Figure 4.9: NEDC battery SOC profile of the torque split imposition model.

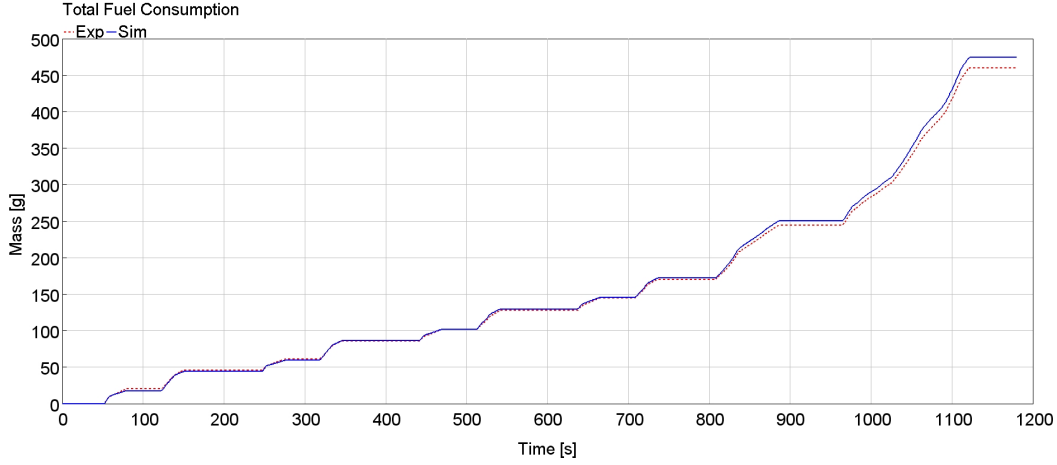


Figure 4.10: NEDC cumulative fuel consumption profile of the split imposition model.

**ICE Torque Profile Imposition Model:** In this model the experimental ICE torque profile is imposed. As advantage, the ICE torque is exactly the measured one, promoting an optimal  $\text{CO}_2$  emissions simulation, but as drawback the experimental measured ICE torque is just an estimation by the vehicle ECU, thus generally less accurate than the EM torque measurement. In this model, a simple hybrid mode bypass is applied forcing the parallel mode for positive ICE torque values, leaving to the Simulink control logic the decisions related to the other operative conditions (e.g. engine cranking, regenerative braking, etc.). Again, the speed trace in figure 4.11 is perfectly followed since the EM provides the torque needed to fill the gaps related to the mismatch between the driver torque demand and the total experimental torque measured.

The simulated ICE torque profile in figure 4.12 is exactly the experimental one, meaning a good feedback of the controls. The simulated EM torque profile in figure 4.13 is similar to the experimental one but for some spikes, related to the

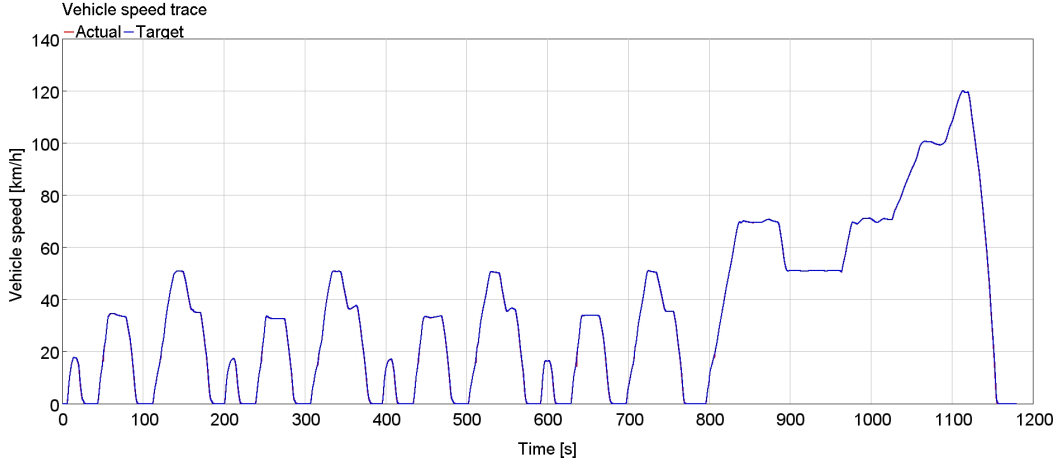


Figure 4.11: NEDC speed trace profile of the ICE torque imposition model.

gear shifting events, remembering that the EM must compensate the torque gaps due to the torque demand discrepancy.

The battery SOC simulated is compared to the experimental values in figure 4.14.

The accuracy of the simulated ICE torque and rotational speed allows an optimal calculation of the engine fuel consumption, thus the CO<sub>2</sub> emissions. The simulated fuel consumption cumulative in figure 4.15, in fact, is overlapping the experimental one, leading to a closely perfect matching.

**EM Torque Profile Imposition Model:** In this model the experimental EM torque profile is imposed. As advantage, the EM torque measured is generally easier to be evaluated compared to the ICE torque, but the drawbacks are related to a more difficult control logic related to compensate the experimental-simulated torque demand gap. In fact, since the total torque requested is higher than the experimental one, the torque provided by the EM during the pure electric mode is not sufficient to let the driver follow the

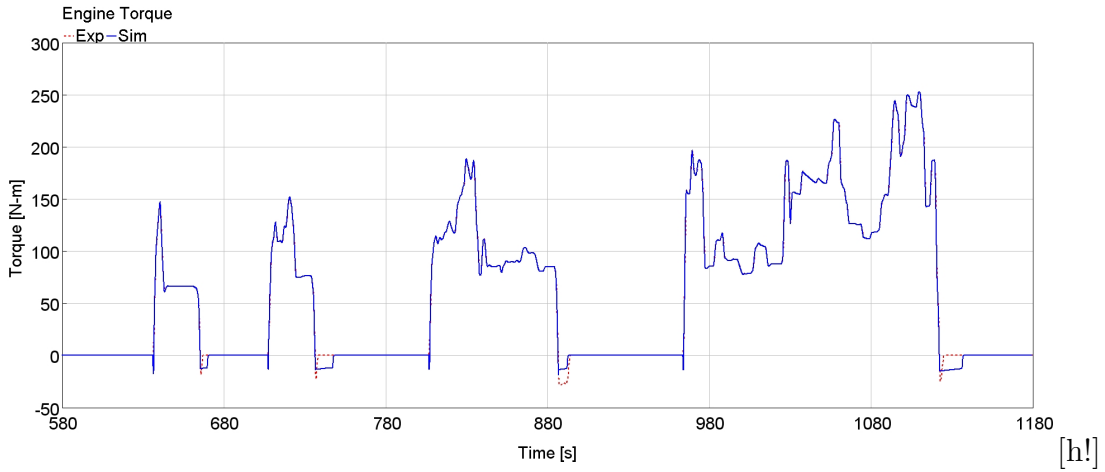


Figure 4.12: NEDC Engine torque profile of the ICE torque imposition model.

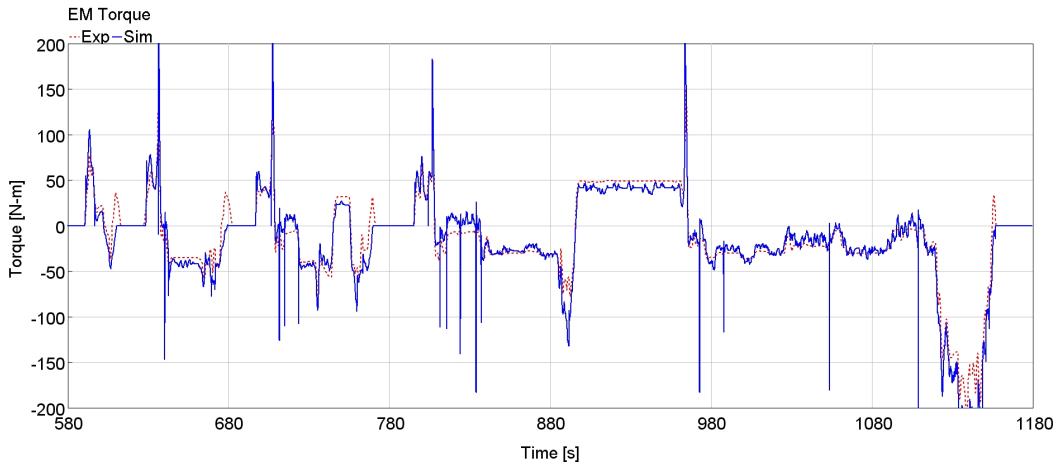


Figure 4.13: NEDC EM torque profile of the ICE torque imposition model.

speed trace properly. Although the speed trace is followed during the parallel mode, when the ICE can compensate the torque gaps, is not followed during pure electric mode. Some controls can still be implemented to avoid the lack of torque in the full electric mode. The one used for this model imposes the torque developed by the EM equal to the total torque demanded by the driver during the full electric mode, regardless the experimental imposed profile. With this type of control the driver can follow the speed profile in figure

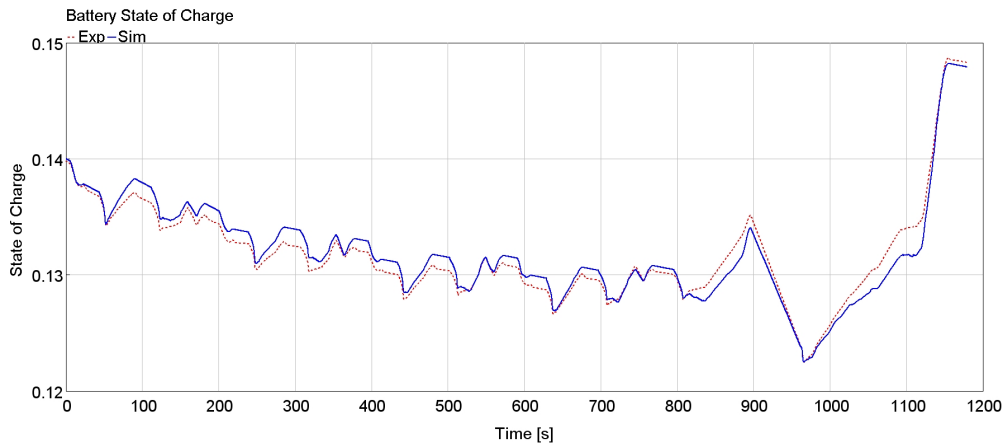


Figure 4.14: NEDC battery SOC profile of the ICE torque imposition model.

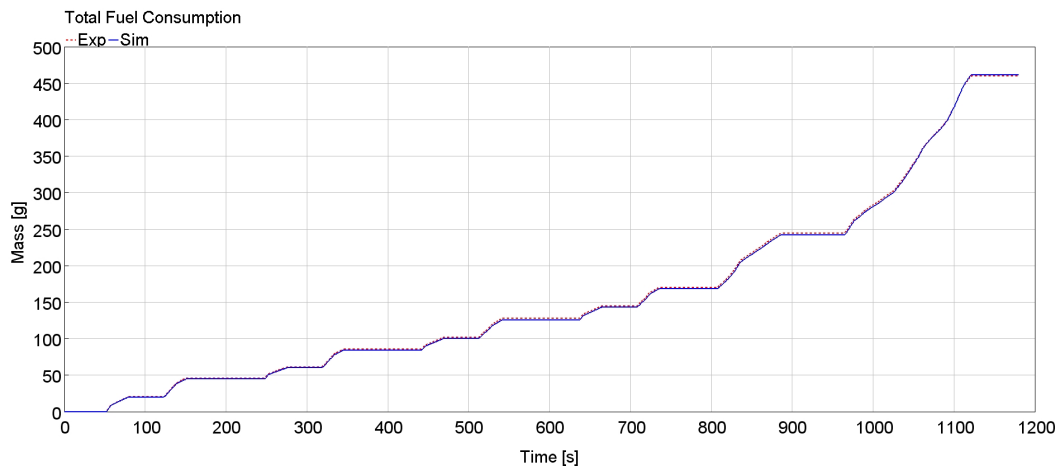


Figure 4.15: NEDC cumulative fuel consumption profile of the ICE torque imposition model.

4.16, although some minor divergences.

Nevertheless, the control implemented for the EM is not sufficient to obtain satisfying results in terms of torque profiles. To overcome this problem, the experimental ICE torque profile is used combined with the experimental engine rotational speed to define whether the vehicle goes in parallel mode, obtaining a profile used to bypass the ECU control logic. The results are quite satisfying:

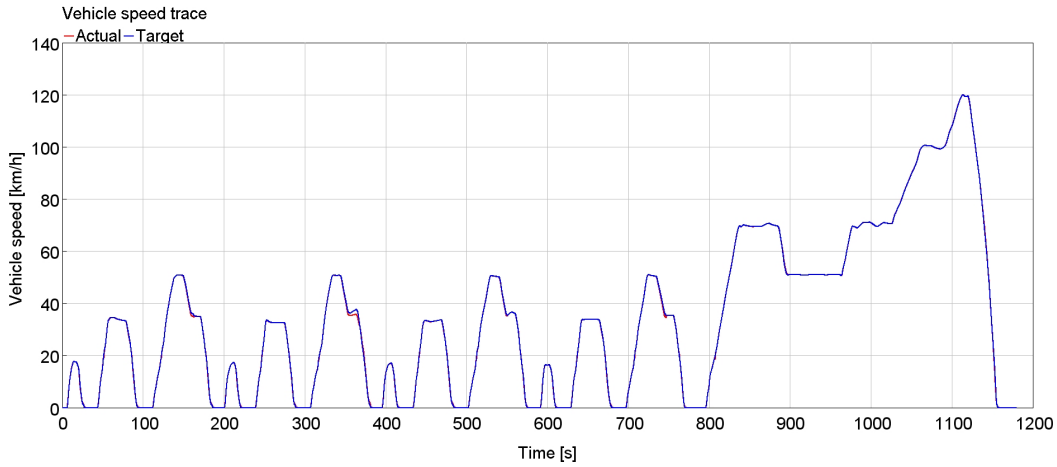


Figure 4.16: NEDC speed trace profile of the EM torque imposition model.

the ICE and EM torques are represented in figures 4.17 and 4.18, meanwhile the simulated battery SOC is the one of figure 4.19.

As predictable, the ICE torque is higher compared to the experimental values due to the compensation effort. The EM torque, instead, follows perfectly the experimental profile but for the pure electric zones in which has to deliver more torque to satisfy the driver requirements according to the type of control implemented. The fuel consumption cumulative in figure 4.20 highlights a trend of overestimation of the consumptions, matching the simulated ICE torque profile.

**Summary results** Defined the compliancy of all the models to the speed trace, the results in terms of CO<sub>2</sub> specific emission calculations are proposed in table 4.1. Although the EM profile and the torque split imposition models show an acceptable error, the ICE torque profile imposition model error is far better than the others. Thus, the ICE torque imposition model will be developed for the simulation of the WLTP and RDE emissions.

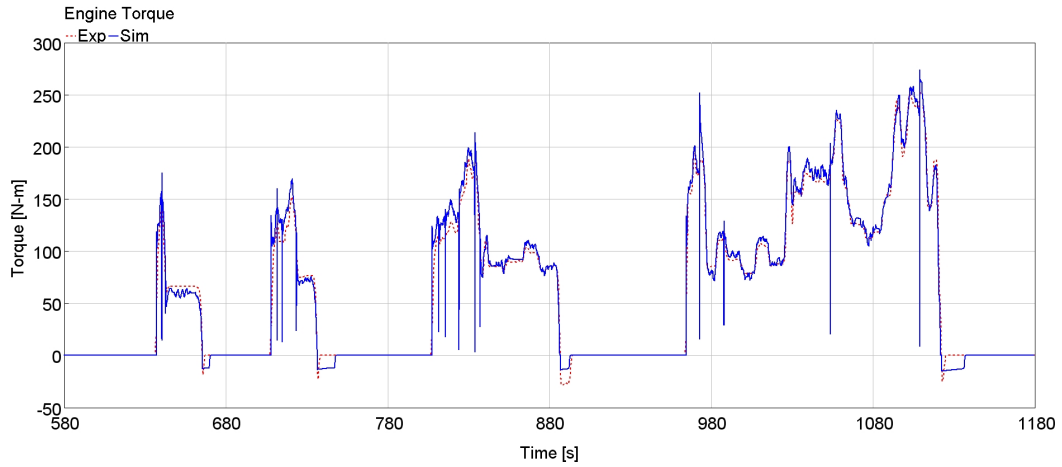


Figure 4.17: NEDC Engine torque profile of the EM torque imposition model.

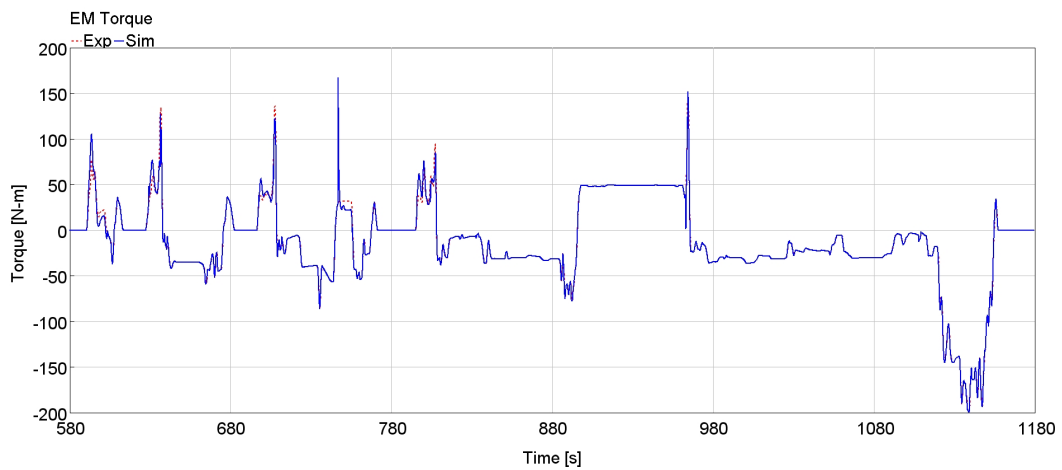


Figure 4.18: NEDC EM torque profile of the EM torque imposition model.

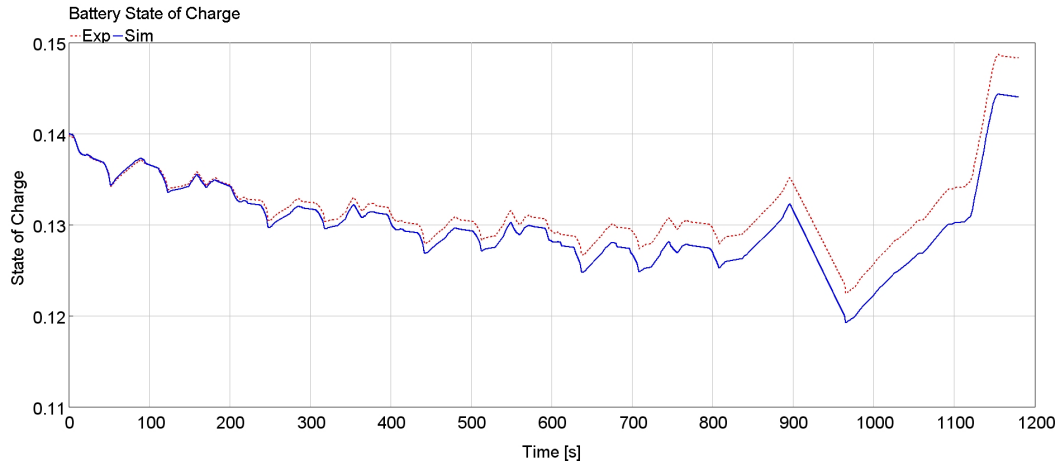


Figure 4.19: NEDC battery SOC profile of the EM torque imposition model.

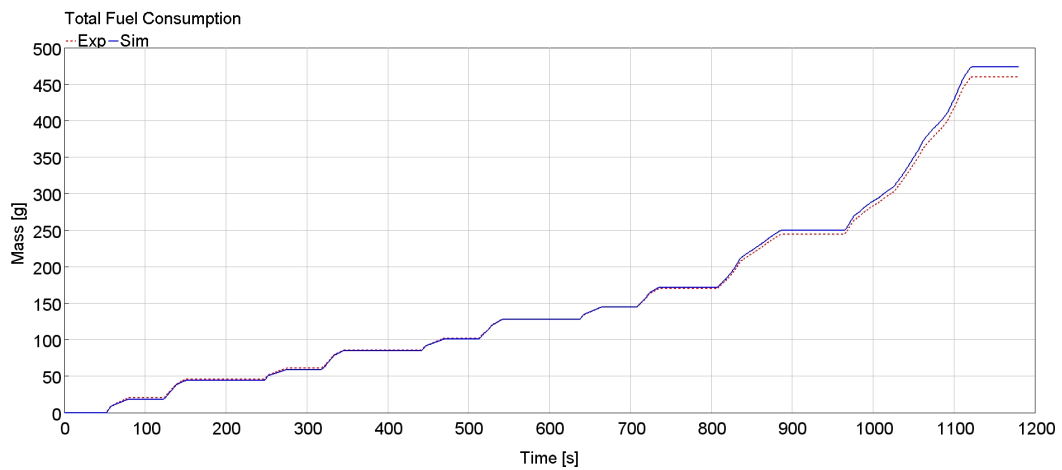


Figure 4.20: NEDC cumulative fuel consumption profile of the EM torque imposition model.

Model	CO <sub>2</sub> Exp specific emissions [g/km]	CO <sub>2</sub> Sim specific emissions [g/km]	Error [%]
Split Imposition	131	135	3.2
ICE Torque Profile Imposition	131	131	0.4
EM Torque Profile Imposition	131	135	2.9

Table 4.1: Summary results of all the models for the NEDC simulation.

#### 4.4.2 WLTP simulation

The model developed in paragraph 4.4.1 related to the imposition of the ICE torque profile is considered and adapted to perform the WLTP simulation. Concerning the gap between the simulated driver torque demand and the experimental one in figure 4.21, it seems to be reduced but still present.

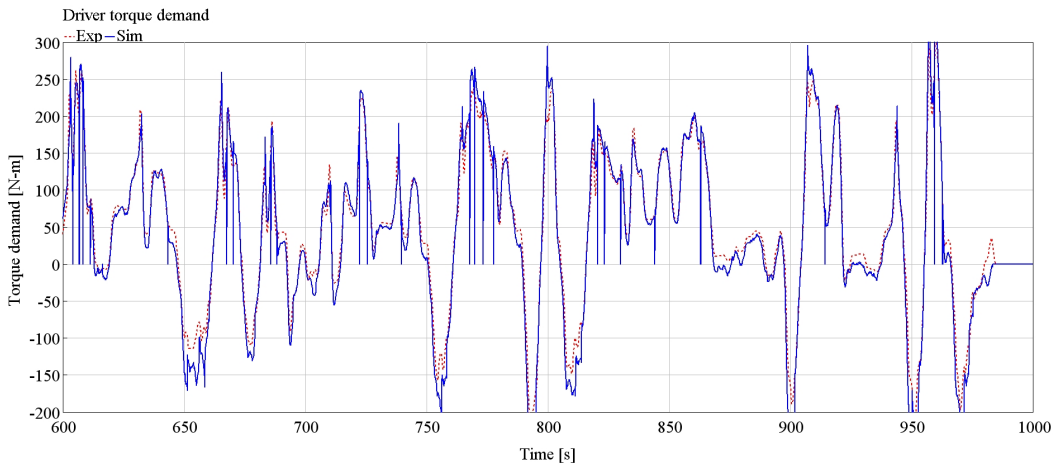


Figure 4.21: WLTP Driver Torque Demand.

The controls implemented for the WLTP are the same of the NEDC, modifying the switch profile and all the parameters related to the cycle ( e.g. the speed

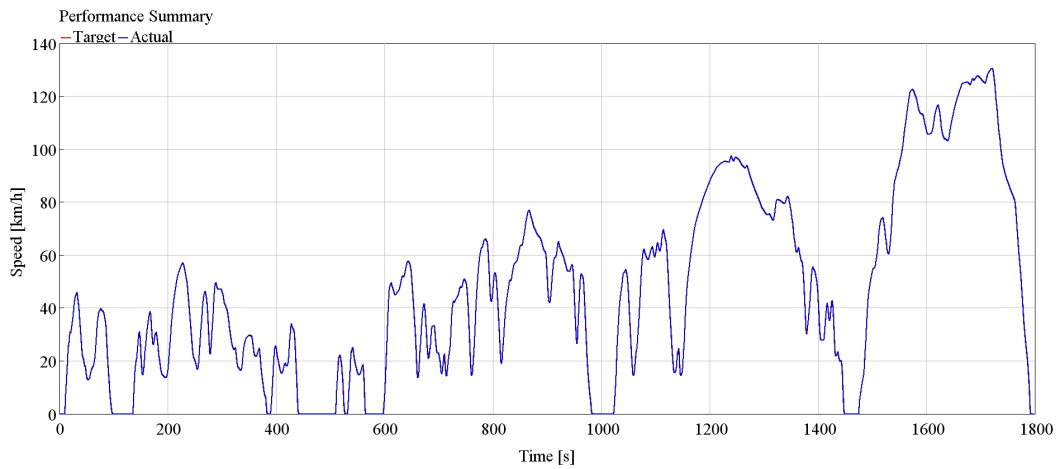


Figure 4.22: WLTP speed trace profile.

trace, gear shift profile, RL coefficients, etc.). Even in this case, the driver is able to perfectly follow the speed trace, according to figure 4.22.

Again, the ICE and EM torque, along with the engine speed, properly follow the experimental profiles in figures 4.23, 4.24, and 4.25.

In figure 4.26, instead, the trend of the battery State of Charge is shown. The divergency of the SOC profiles is quite inevitable since the torque gap between simulated and experimental driver demand is compensated by a more intense use of the EM. A relatively good signal, instead, is given by the fact that the profiles present just an offset and do not show changes in the trend.

Despite a minor error, reported in table 4.2, the simulated cumulative fuel consumption profile show a good match even if the model overestimates the emissions, as showed in figure 4.27.

Since the model is map based and the only parameters that affect the engine fuel consumption are the engine bmep and speed, a deeper analysis of the factors leading to higher CO<sub>2</sub> emissions is needed and performed considering the simulated instantaneous fuel consumption compared to the experimental

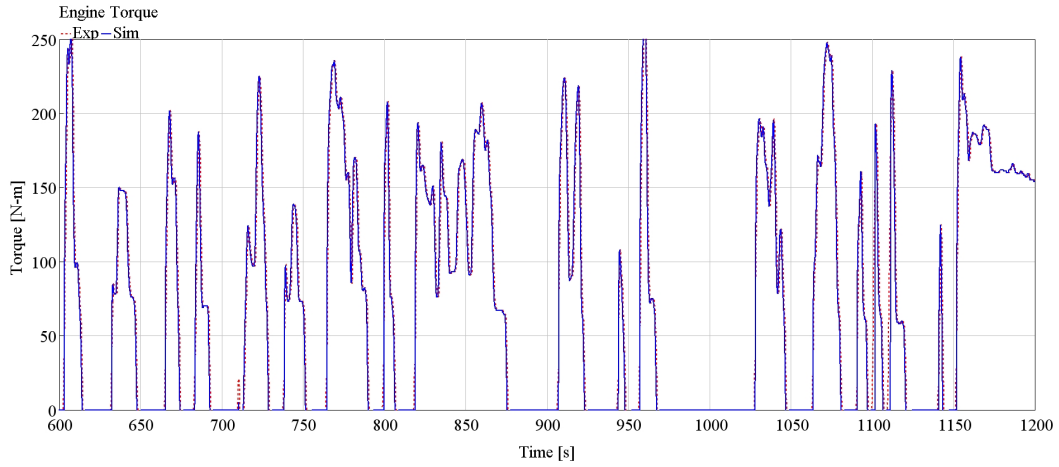


Figure 4.23: WLTP Engine Torque profile.

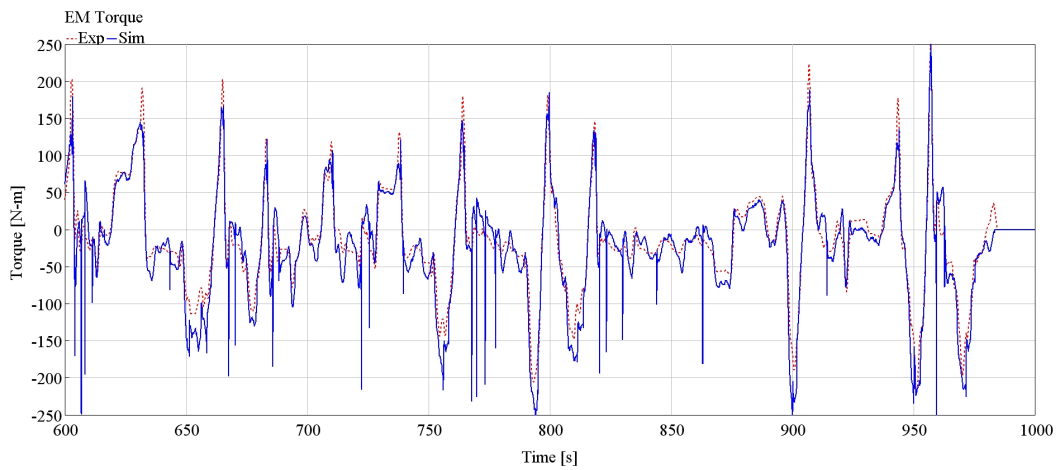


Figure 4.24: WLTP EM Torque profile.

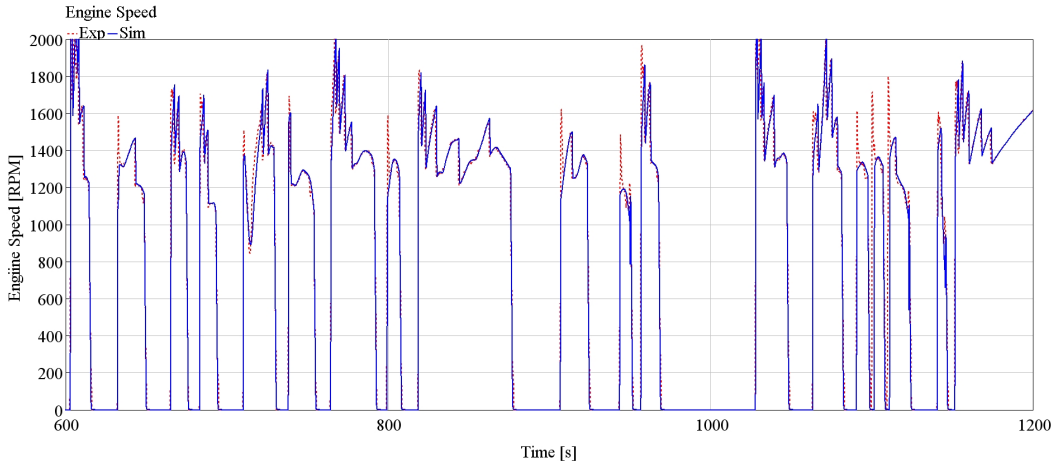


Figure 4.25: WLTP engine speed profile.

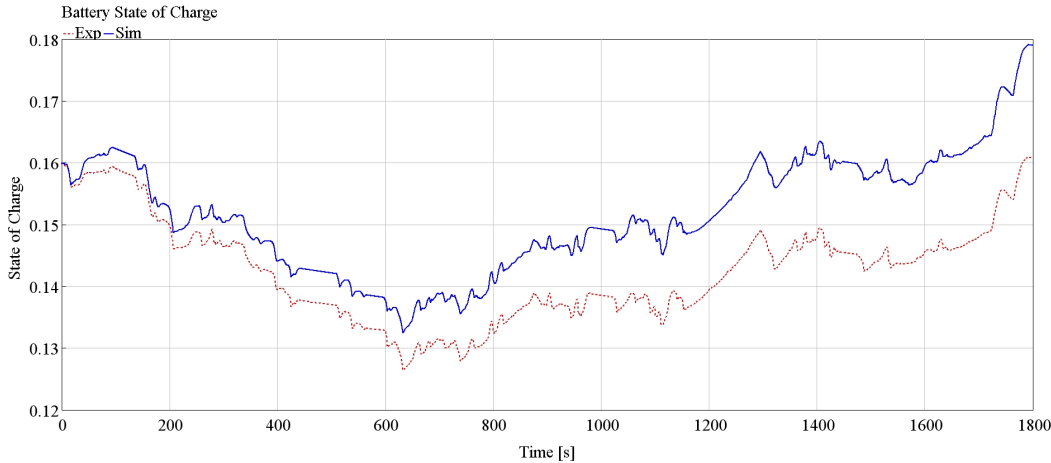


Figure 4.26: WLTP battery SOC profile.

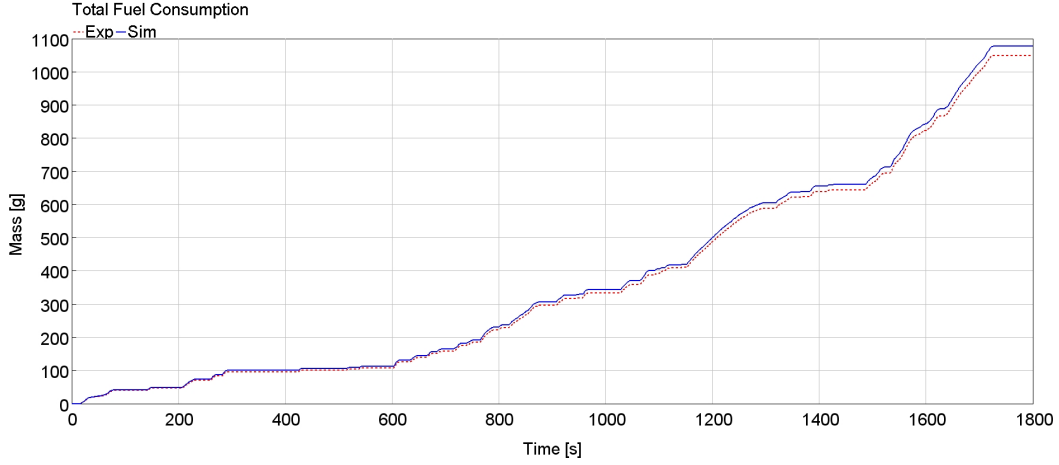


Figure 4.27: WLTP cumulative fuel consumption profile.

values in figure 4.28.

In the interval 700s-800s the cumulative CO<sub>2</sub> emission difference raises from 21g to 27g. In most of this interval, the instantaneous simulated fuel rate is higher compared to the experimental one and this could be addressed to the experimental maps used for the model.

CO <sub>2</sub> Exp specific emissions [g/km]	CO <sub>2</sub> Sim specific emissions [g/km]	Error [%]
141	146	3.0

Table 4.2: Results of the model for the WLTP simulation.

### 4.4.3 RDE simulation

In line with the simulations carried out for the NEDC and WLTP procedures, also the model used for the RDE simulation imposes the ICE torque profile. Since this test is performed on road and not on chassis dyno, the road elevation recorded by the PEMS GPS in figure 4.29 is added.

The model’s speed trace in figure 4.30 is perfectly followed. The torque profiles

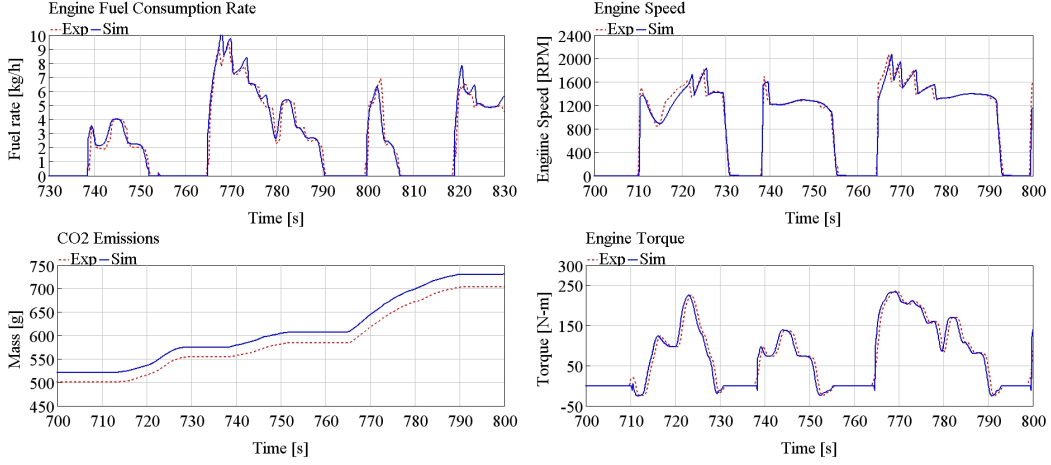


Figure 4.28: WLTP parameter comparison.

are presented in figures 4.31 and 4.32.

The ICE torque profiles are perfectly overlapped, leading to a fuel consumption cumulative in figure 4.33 that quite overlaps the experimental values. The EM torque profile, instead, is much more volatile than the experimental one.

Even the SOC profile trend is good compared to the experimental one, as showed in figure 4.34.

CO <sub>2</sub> Exp specific emissions [g/km]	CO <sub>2</sub> Sim specific emissions [g/km]	Error [%]
91	92	0.9

Table 4.3: Results of the model for the WLTP simulation.

The result of the simulation in table 4.3, in terms of specific emissions, define an error of less than 1% compared to the experimental value.

## CHAPTER 4. TEST CYCLE SIMULATION

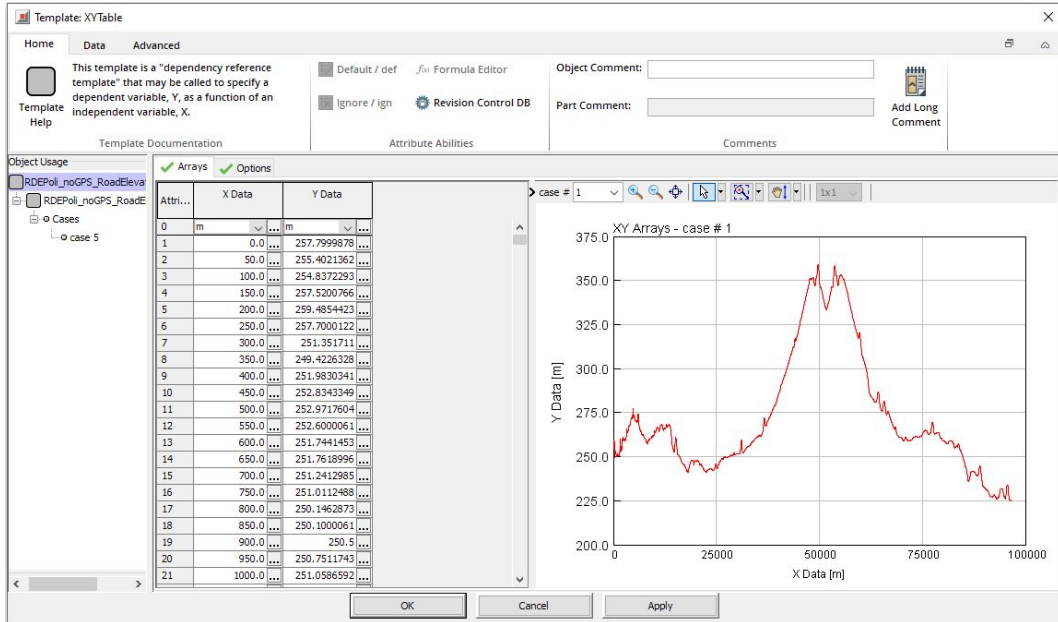


Figure 4.29: RDE GPS road elevation profile.

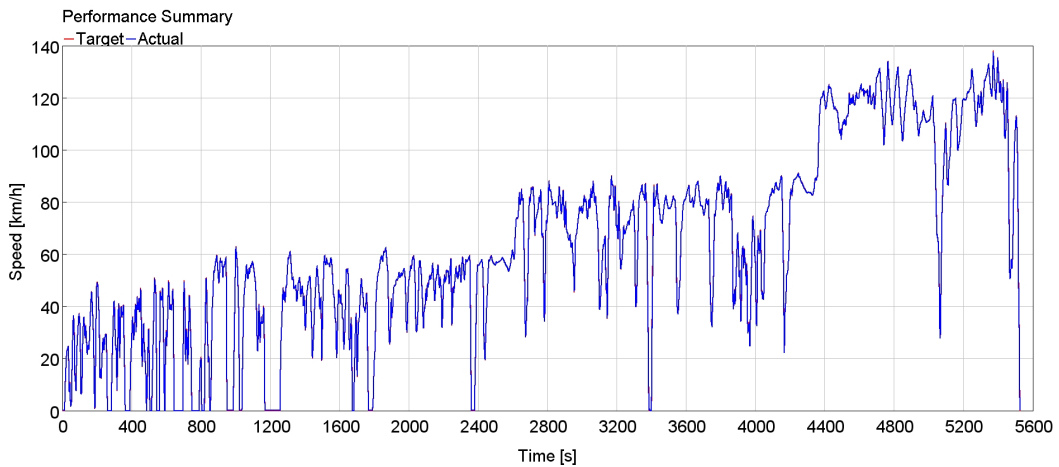


Figure 4.30: RDE speed trace profile.

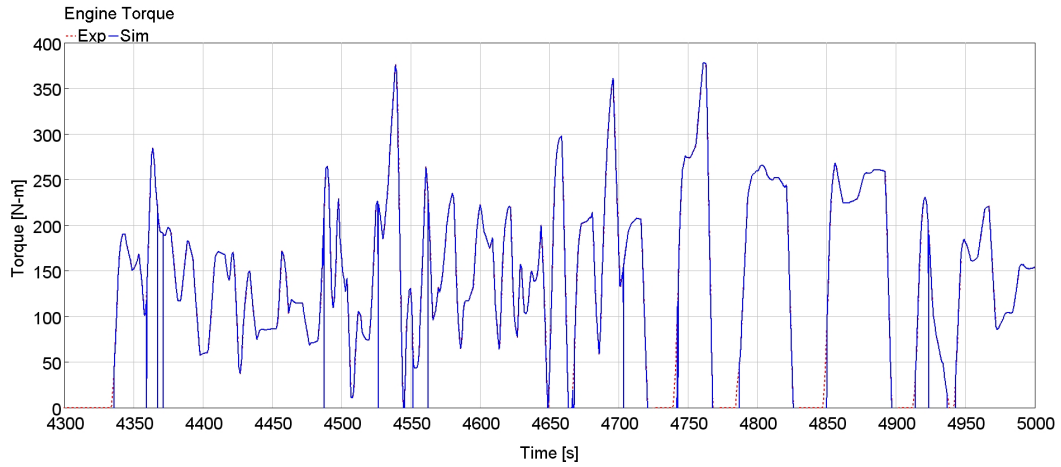


Figure 4.31: RDE Engine Torque profile.

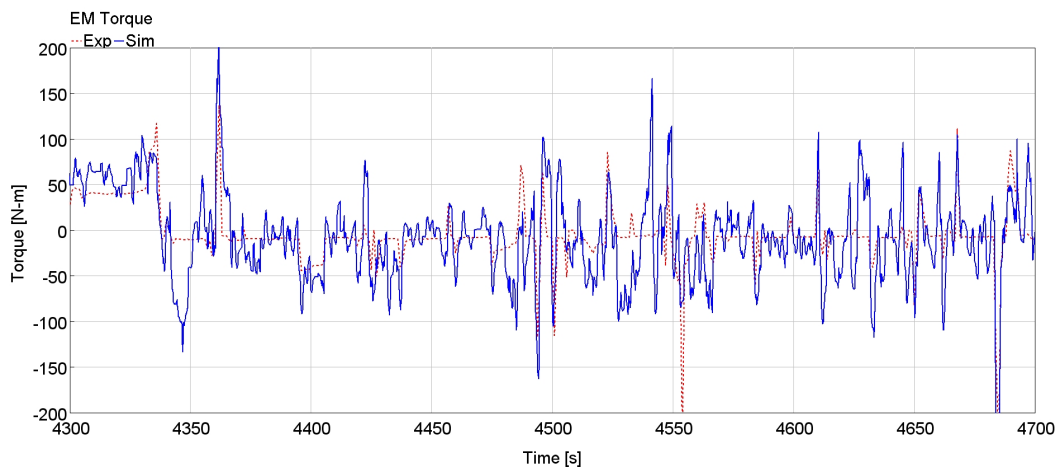


Figure 4.32: RDE EM Torque profile.

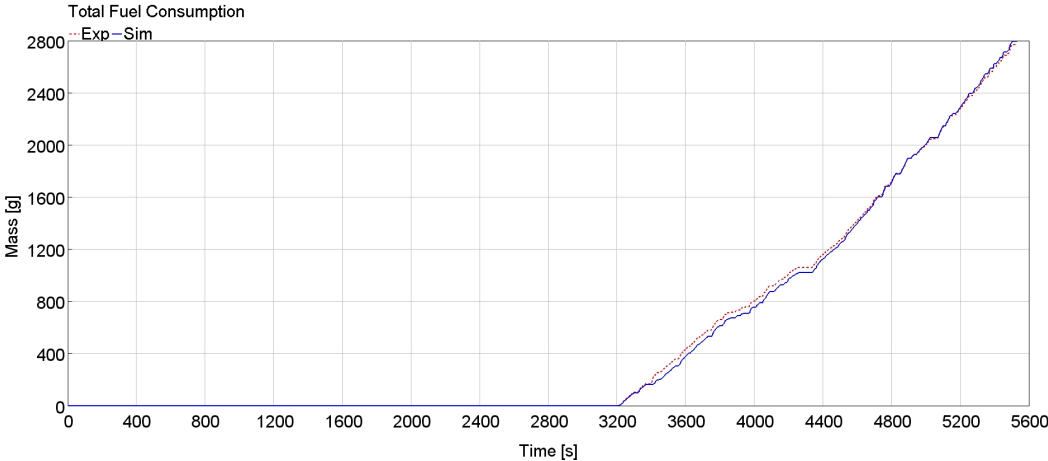


Figure 4.33: RDE fuel consumption cumulative.

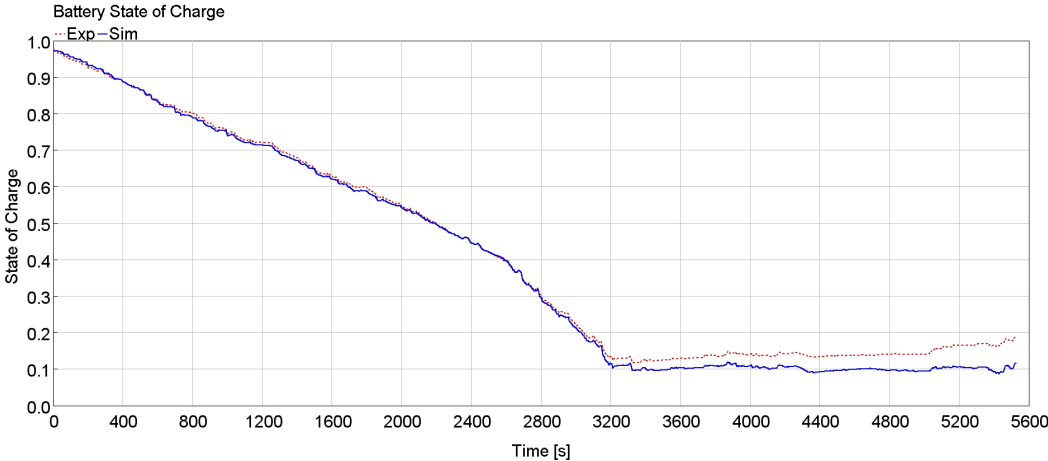


Figure 4.34: RDE SOC profile.

# Chapter 5

## Conclusions

The increasing demand for a more effective control on pollutant and CO<sub>2</sub> emissions led to the definition of a new type approval procedure that combines the laboratory testing with the on-road one. The aim of this work was to analyse the new procedure both by the legislation and practical assessing point of view. In the second chapter, the differences between the TA procedures have been highlighted and the boundary conditions for a RDE compliance test have been defined, obtaining a good overview of all the test requirements.

In the third chapter, the PEMS instrumentation needed for the RDE onset, along with the practical difficulties and procedures for the test assessment, have been investigated, and some examples of not-valid RDE tests have been presented.

In the fourth chapter the possibility of the reproduction of CO<sub>2</sub> emissions during an experimental RDE test cycle through numerical simulation is investigated. The emissions, obtained through the imposition of the experimental ICE torque profile, show encouraging results, proving the possibility to obtain

accurately calibrated models even for hybrid vehicles.

As future development, a model can be obtained imposing the hybrid control logic of the vehicle and a RDE compliant route could be generated through tools such as GT's Virtual RDE (vRDE) to define the vehicle's emissions prior to the on-road testing.

This work was intended to be a comprehensive description of the RDE legislation. In the future the boundary conditions could change, or the technologies used for the test assessment evolve. Nevertheless, the RDE type approval procedure is proven to properly fill the gap with real driving emissions, although the difficulties related to its assessment.

# Bibliography

- [1] IEA, “Tracking transport 2020.” <https://www.iea.org/reports/tracking-transport-2020>, May 2020.
- [2] P. M. et al., “From laboratory to road,” tech. rep., ICCT, 2014.
- [3] A. Ramos, J. Muñoz, F. Andrés, and O. Armas, “Nox emissions from diesel light duty vehicle tested under nedc and real-word driving conditions,” *Transportation Research Part D: Transport and Environment*, vol. 63, pp. 37–48, 2018.
- [4] Horiba, “Real driving emissions.” <https://www.horiba.com/horiba/automotive-test-systems/real-driving-emissions/>.
- [5] Delphi, “Worlwide emissions standards - passenger cars and light duty vehicles,” 2017.
- [6] G. DiPierro, E. Galvagno, G. Mari, F. Millo, M. Velardocchia, and A. Perazzo, “A reverse-engineering method for powertrain parameters characterization applied to a p2 plug-in hybrid electric vehicle with automatic transmission,” tech. rep., SAE Technical Paper, 2020.

- [7] F. Millo, L. Rolando, and M. Andreatta, “Numerical simulation for vehicle powertrain development,” in *Numerical Analysis-Theory and Application*, IntechOpen, 2011.
- [8] J. E. Jonson, J. Borken-Kleefeld, D. Simpson, A. Nyíri, M. Posch, and C. Heyes, “Impact of excess nox emissions from diesel cars on air quality, public health and eutrophication in europe,” *Environmental Research Letters*, vol. 12, no. 9, p. 094017, 2017.
- [9] J. M. Luján, A. García, J. Monsalve-Serrano, and S. Martínez-Boggio, “Effectiveness of hybrid powertrains to reduce the fuel consumption and nox emissions of a euro 6d-temp diesel engine under real-life driving conditions,” *Energy Conversion and Management*, vol. 199, p. 111987, 2019.
- [10] G. DiPierro, F. Millo, C. Cubito, B. Ciuffo, and G. Fontaras, “Analysis of the impact of the wltc procedure on co<sub>2</sub> emissions of passenger cars,” tech. rep., SAE Technical Paper, 2019.
- [11] J. Ko, D. Jin, W. Jang, C.-L. Myung, S. Kwon, and S. Park, “Comparative investigation of nox emission characteristics from a euro 6-compliant diesel passenger car over the nedc and wltc at various ambient temperatures,” *Applied energy*, vol. 187, pp. 652–662, 2017.
- [12] A. Dimaratos, D. Tsokolis, G. Fontaras, S. Tsiakmakis, B. Ciuffo, and Z. Samaras, “Comparative evaluation of the effect of various technologies on light-duty vehicle co<sub>2</sub> emissions over nedc and wltc,” *Transp. Res. Procedia*, vol. 14, pp. 3169–3178, 2016.

- [13] R. A. Varella, M. V. Faria, P. Mendoza-Villafuerte, P. C. Baptista, L. Sousa, and G. O. Duarte, “Assessing the influence of boundary conditions, driving behavior and data analysis methods on real driving co2 and nox emissions,” *Science of the Total Environment*, vol. 658, pp. 879–894, 2019.
- [14] T. Bodisco and A. Zare, “Practicalities and driving dynamics of a real driving emissions (rde) euro 6 regulation homologation test,” *Energies*, vol. 12, no. 12, p. 2306, 2019.
- [15] N. F. González, J. C. Kindelán, J. M. L. Martí, *et al.*, “Methodology for instantaneous average exhaust gas mass flow rate measurement,” *Flow Measurement and Instrumentation*, vol. 49, pp. 52–62, 2016.
- [16] G. Ferrari, *Motori a combustione interna*. Società Editrice Esculapio, 2016.
- [17] T. Incorporated, “Choosing the right cpc for your application,” August 2015.
- [18] M. Ahmadinejad, M. R. Desai, T. C. Watling, and A. P. York, “Simulation of automotive emission control systems,” *Advances in Chemical Engineering*, vol. 33, pp. 47–101, 2007.
- [19] S. W. Duym, “Simulation tools, modelling and identification, for an automotive shock absorber in the context of vehicle dynamics,” *Vehicle System Dynamics*, vol. 33, no. 4, pp. 261–285, 2000.